2018-05-01

Constraining Kura and South Caspian Basin Maikop Source Rock Stratigraphy, Deposition, and Timing Using Chemostratigraphy of Redox-Sensitive Metals and Re-Os Geochronology

Alex M. Washburn
Brigham Young University

Constraining Kura and South Caspian Basin Maikop Source Rock Stratigraphy, Deposition, and Timing Using Chemostratigraphy of Redox-Sensitive Trace Metals and Re-Os Geochronology

Alex M. Washburn

A thesis submitted to the faculty of
Brigham Young University
in partial fulfillment of the requirements for the degree of

Master of Science

Samuel M. Hudson, Chair
Scott Ritter
Thomas Morris

Department of Geological Sciences

Brigham Young University

ABSTRACT

Constraining Kura and South Caspian Basin Maikop Source Rock Stratigraphy, Deposition, and Timing Using Chemostratigraphy of Redox-Sensitive Trace Metals and Re-Os Geochronology

Alex M. Washburn
Department of Geological Sciences, BYU
Master of Science

The Oligocene-Miocene Maikop Series in the South Caspian and Kura Basins is the key petroleum source rock for both offshore and onshore petroleum development in Azerbaijan. The Maikop is a thick (up to 3 km) succession of silty mudstones containing up to 15% total organic carbon (TOC), but is greatly lacking diagnostic microfaunal assemblages useful for dating and stratigraphically constraining the deposition of the mudstone. Current stratigraphic constraints relying on microfaunal assemblages, radiostratigraphy, and chemostratigraphy are robust, but key information is still missing. This study adds numerical age data to Maikop stratigraphy through Re-Os geochronology. Of five sample suites analyzed from the Kura Basin of eastern Azerbaijan, one Re-Os data set produced significant range in $^{187}Re/^{188}Os$ vs $^{187}Os/^{188}Os$ space to yield an isochron of 17.2 ± 3.2 Ma. Other sample suites yield imprecise Re-Os age constraints as a result of variable initial $^{187}Os/^{188}Os$ values and limited range in $^{187}Re/^{188}Os$ vs $^{187}Os/^{188}Os$ space. The initial $^{187}Os/^{188}Os$ values of these data sets were compared with the known $^{187}Os/^{188}Os$ of seawater values for the past 70 million years to provide the best qualitative age constraints. Pre-Maikopian strata studied at Perikeshkul was found to coincide in $^{187}Os/^{188}Os$ values with the Eocene-Oligocene Transition (EOT) Os excursion, indicating deposition initiation of Maikopian strata following the EOT. Preservation of organic matter in intervals with initial $^{187}Os/^{188}Os$ values that deviate significantly from global $^{187}Os/^{188}Os$ values indicate basin restriction and the development of anoxia. High Os abundances, enrichment in detrital elements Al, Ti, Ga, Sc, and La, and changing basin circulation during the deposition of Maikop strata at 17.2 Ma may indicate the initial episodic uplift of the Greater Caucasus Mountains, changes in sediment provenance, or changing proximity to sediment source.

Keywords: Paratethys, source rock, chemostratigraphy, geochronology, Maikop

ACKNOWLEDGEMENTS

I am grateful first and foremost to my wonderful wife Rachel and daughter Taylor, without whom I would not have purpose. Special thanks goes to Dr. Sam Hudson who has been both an encouraging advisor and a loyal friend; without him, none of the work represented in this thesis would have come to be. Sam made this work an experience in the endeavors of human curiosity that has fueled me to continue in the work. I am also especially grateful to Dr. Dave Selby who, despite long distance and limited contact, offered kindly tutelage, constructive criticism, and valuable insight. I am also indebted to him and his research staff for allowing me the opportunity to work in their labs at Durham University, where I was able to learn the precise details of the most terrifyingly delicate chemistry analysis I have ever taken part in. I am very grateful to have been able to learn so much under their patient assistance. I would also like to express my gratitude to my committee members, Dr. Scott Ritter and Dr. Tom Morris for their assistance in supporting, reviewing, and editing the research that I was able to perform. In addition to my committee members, I am also grateful to the entire staff of BYU, particularly Kevin Rey and Dave Tingey for their laboratory assistance, especially in determining the best methods for analyzing for metals not typically analyzed in these labs. Lastly, I want to thank the South Caspian Group of BP for their generous funding in making this project possible. In particular, I want to thank Nazim Abdullayev and Nataliya Shiyanova for their assistance in field work and the process of editing this manuscript.

TABLE OF CONTENTS

LIST OF FIGURES

LIST OF TABLES

Introduction

Understanding the evolution of the ancient Paratethys Sea is critical in resolving the formation of petroleum system elements in its sedimentary basins, including the South Caspian and Kura Basins of eastern Azerbaijan. Important events in the evolution of the Paratethys Sea include the restriction of the Paratethys from open-marine circulation and the emergence of the Greater Caucasus Mountains as a result of collisional tectonics. A key to understanding these events in the Paratethys Sea lies within the deposits of the Maikop Series in eastern Azerbaijan. The Maikop Series is thought to have been deposited from the latest Eocene throughout the Oligocene and into the Late Miocene (Hudson et al., 2008; Popov et al., 2008; Egan et al., 2009; Van der Boon et al., 2015). Several methods have previously been used to stratigraphically and geochronologically constrain the Maikop Series to unlock clues pertaining to the isolation of the Paratethys Sea, including biostratigraphy, radiostratigraphy, and chemostratigraphy. These methods have thus far greatly added to the resolution of paleogeographic evolutionary events, but key information is still missing. The purpose of this study is to constrain the depositional ages of key intervals of the Maikop in eastern Azerbaijan through the application of Re-Os isotope geochronology. Furthermore, this study will discuss elemental analysis on redox-sensitive metals, total organic carbon (TOC), kerogen types, and detrital input in an effort to further develop the subaqueous depositional conditions, changing sediment provenance, and the emergence of the Greater Caucasus Mountains.

Geologic Background

The Maikop Series was deposited in the Paratethys Sea, an epicontinental sea that evolved from the unrestricted Tethys Ocean. The Maikop Series was deposited throughout the

ancient Paratethys, making deposits of the Maikop identifiable across an extensive region, from as far west as the Eastern Black Sea and as far north as the northern portion of the central Caspian region (, Green et al., 2009). Due to its association with the Paratethys Sea, the Maikop is often studied to unlock clues pertaining to the evolution of the Paratethys and the factors that affect it, including climate, tectonics, eustacy, etc. (Rogl, 1999; Popov et al., 2008; Hudson et al., 2008; Johnson et al., 2009). A prime area in which to study the Maikop Series is in eastern Azerbaijan, where deposits of the Maikop are abundant in outcrop. Additionally, the South Caspian and Kura Basins of eastern Azerbaijan produce large volumes of hydrocarbons sourced from the Maikop Series (Isaksen et al., 2007; Bechtel et al., 2014), making the study of the Maikop in this area key to understanding organic matter preservation, maturation, and hydrocarbon migration associated with these accumulations.

The Paratethys Sea is thought to have formed either during the Paleocene and Eocene epochs (Gaetani & Garzanti, 1991; Golonka, 2004; Kaz'min & Tikhonova, 2005), or later near the Eocene/Oligocene boundary (Popov et al., 1993; Rogl, 1999). Upon initial formation of the Paratethys, open seaways existed to the west and possibly to the east (Figure 1). These open seaways affected the chemistry of Paratethys waters by allowing communication and circulation of oxidized water with the open ocean. Throughout the Oligocene and Miocene epochs, it is thought that these open seaways underwent periodic closure due to either global eustacy or collisional tectonics before becoming completely closed off later during the Late Miocene (Popov et al, 2008; Hudson et al., 2008; Johnson et al., 2009).

A primary basin of interest in the Paratethys Sea is the South Caspian Basin (SCB), known for its unique structural characteristics and prolific hydrocarbon production (Figure 2).

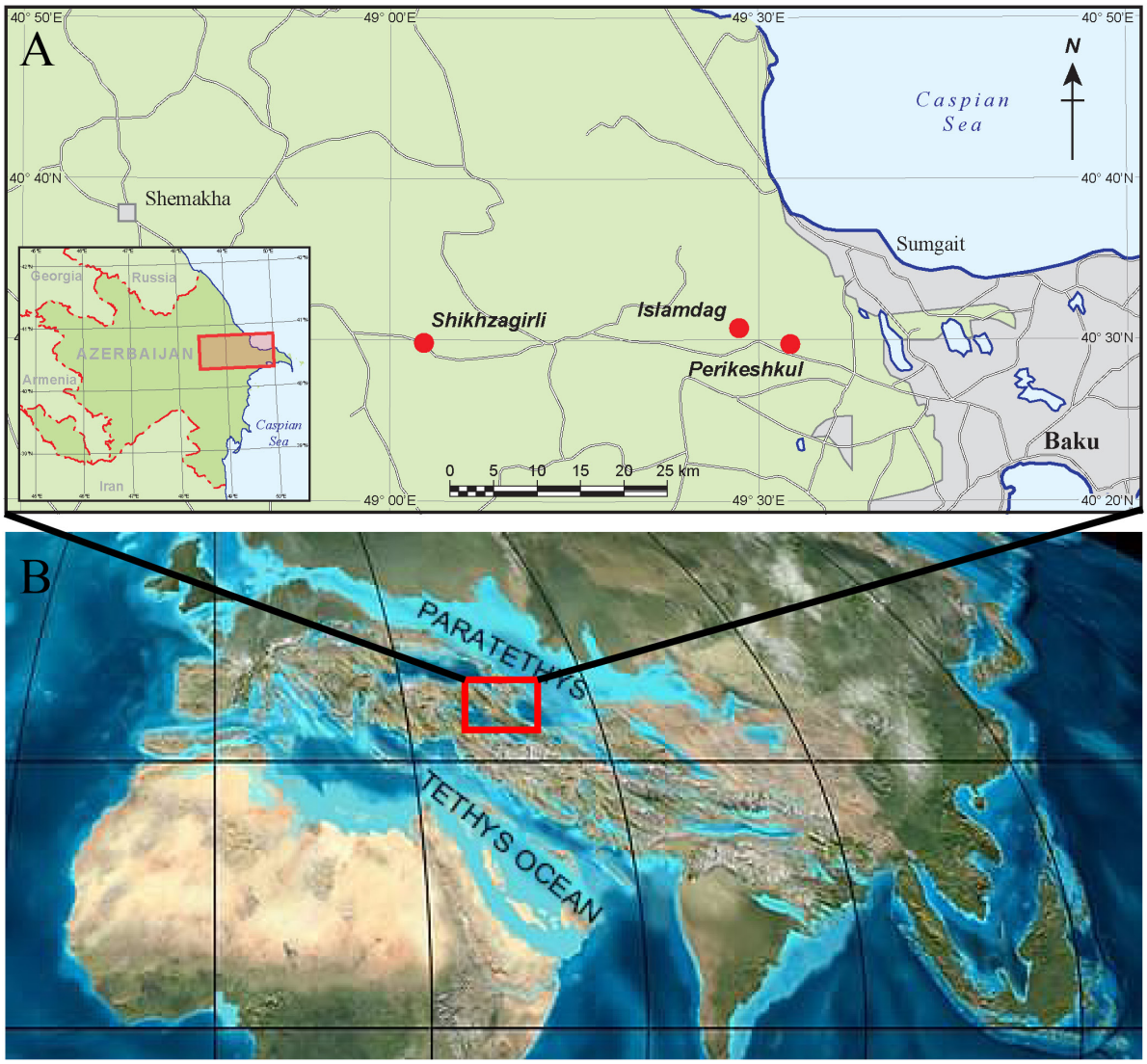

Figure 1 - (A) Modern geographical map displaying the location of the field area, with the three sample sites marked with red dots. Map modified from Hudson et al., 2008. (B) Paleogeographic representation of the Paratethys Sea region during the Eocene-Oligocene, with the study area outlined in red. Map modified from Blakey, https://www2.nau.edu/rcb7/.

The SCB opened as part of a back-arc basin that formed sometime during the Mid-Jurassic to Cretaceous Period as a result of long-lived northward subduction of the Neo-Tethys (Dercourt et al. 1986; Zonenshain & Le Pichon 1986; Granath & Baganz 1996; Otto 1997; Nikishin et al. 1998; Granath et al. 2000; Stampfli et al. 2001; Ziegler et al. 2001; Brunet et al. 2003). The SCB basement is thought to be oceanic crust, which lies at a depth of 20-25 kilometers (Dewey et al. 1973; Berberian 1983; Zonenshain & Le Pichon 1986; Priestley et al. 1994; Brunet et al. 2003).

Due to the great depth of the basin, no borehole penetrations to the basement exist, and continuous seismic correlation is lacking (Brunet et al., 2003). Early sedimentation in the SCB is highly debated, but the bulk of the sedimentary infill of the SCB is attributed to deposits that are Oligocene and younger (Figure 2, Brunet et al., 2003). Sediment influx to the basin is attributed mainly to three major rivers, the paleo-Volga, Kura, and Amu Darya rivers that carried sediment from as far east as the Himalayas and as far north as Moscow (Figure 1; Allen et al., 2002; Brunet et al., 2003). Rapid sedimentation during the Pliocene to Quaternary deposited more than 10 km of sediment in less than 5 Myr over the Maikop Series, thereby preventing the normal expulsion of fluids. As a result, the Maikop and much of the overlying Productive Series is overpressured and undercompacted (Narimanov, 1993; Brunet et al., 2003).

The Kura Basin (KB) is a sub-basin of the SCB to the west that formed as a flexural basin between the Greater Caucasus to the north and the Lesser Caucasus and Talysh Mountains to the south (Brunet et al., 2002; Kaz'min & Tikhonova, 2006). Studies on the Maikop are generally performed in the Kura Basin where the Maikop is shallower, appearing in outcrop along eastern Azerbaijan (Figure 2; Popov et al., 2008; Hudson et al., 2008; Johnson et al., 2009). The Maikop in the KB is thought to be time correlative to the Maikop in the deep SCB (Johnson et al., 2009).

Though poorly constrained, the onset of Maikop deposition is thought to have occurred during the Late Eocene and continued through the Miocene. Therefore, the Maikop likely recorded events pertaining to SCB and KB tectonics and circulation restriction in its geochemical signature. Restriction of these basins in the Paratethys Sea resulted in the development of suboxic to anoxic conditions at the sediment/water interface, though there are other factors regarding basin dynamics that must be taken into consideration. Furthermore, the Maikop may record the emergence of the Caucasus Mountains, the timing of which is also poorly constrained.

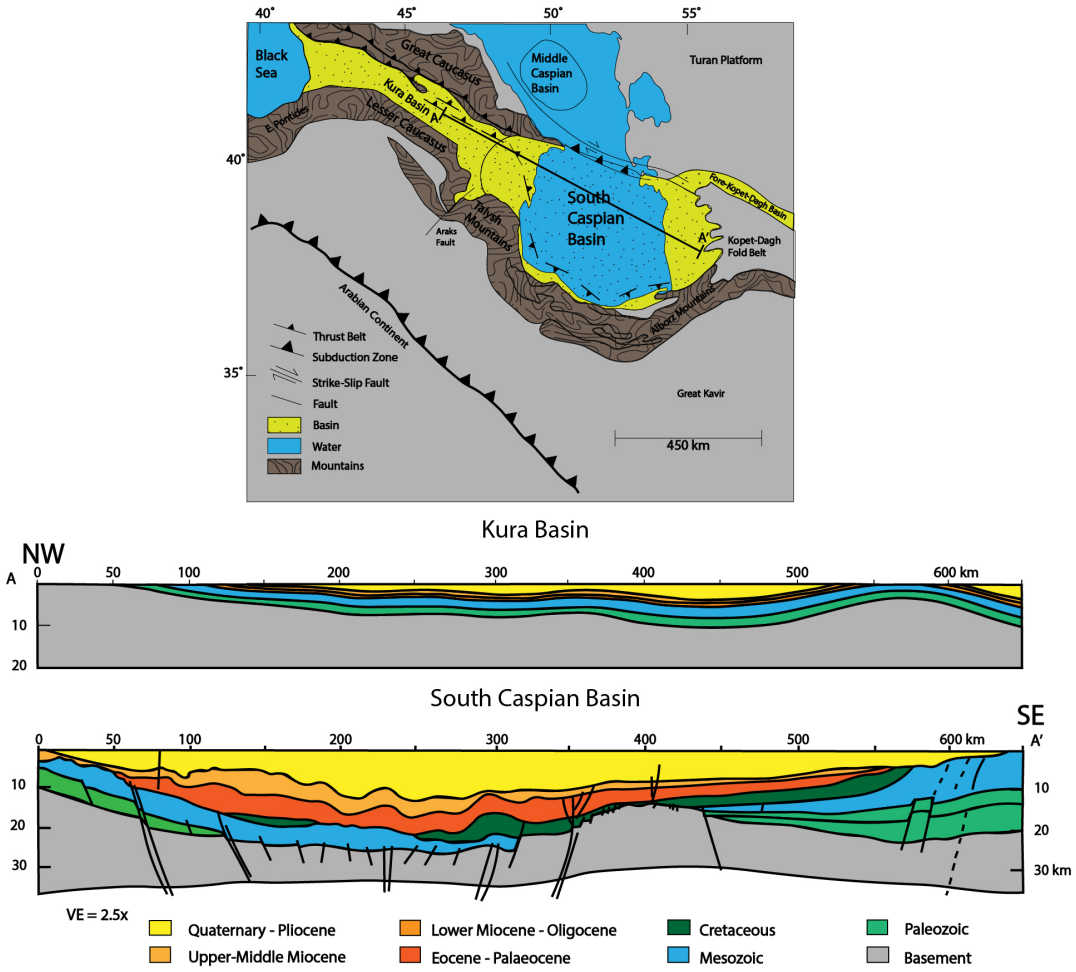

Figure 2 - Modern structural representation of the South Caspian and Kura Basin areas. Collisional tectonics result in a structurally complex area. Cross section A-A' is divided for comparison into two parts: the South Caspian and Kura Basins. Note the depth of relatively young sediment in the SCB, indicating rapid sedimentation that resulted in overpressurized units that make deep drilling hazardous.

Current constraints place the first major uplift of the Greater Caucasus in the Middle Miocene (Ershov et al., 2003; Saintot et al., 2006; Vincent et al., 2007), with widespread compressional deformation in the Greater Caucasus occurring from the Pliocene up into the present (Allen et al., 2003; Green et al., 2009). The emergence of the Greater Caucasus Mountains may be reflected in preserved Maikop strata by an increase of geochemical indicators of detrital influx and restriction (Vincent et al., 2007; Johnson et al., 2009).

The Maikop Series is composed primarily of mudstones largely devoid of diagnostic microfaunal assemblages, making the Maikop notoriously difficult to constrain stratigraphically

and geochronologically. Recent studies have attempted to add stratigraphic resolution by the application of chemostratigraphy, biostratigraphy of nanofossils, and radiostratigraphy (Hudson et al., 2008; Popov et al., 2008; Efendiyeva et al., 2012). It is noted from pyrolysis data that the primary concentration of preserved organic matter exists in the Maikop in thin, discreet intervals of black shale (Hudson et al., 2008). The preservation of the bulk of organic matter in these thin, discreet intervals may correlate to periods of restricted circulation in the Paratethys Sea (Hudson et al., 2008). Preservation of organic matter in sedimentary basins results from deposition of organic matter in suboxic to anoxic reducing environments, followed by sufficiently rapid burial. Restricted circulation resulting from the isolation of the Paratethys would allow for the development of a stagnant, stratified water column that would lead to the development of suboxic to anoxic, reducing conditions.

Deposits of the Maikop vary in thickness regionally. Maikop deposits in the SCB are thickest, ranging up to 3 km thick (Figure 2, cross-section), but are also very deep and are known to be overpressured. Studies on the Maikop in the SCB have been limited to mud volcano ejecta (Isaksen et al., 2007). Maikop deposits thin westward from the SCB into the KB, where onshore deposits of the Maikop may be found in outcrop. Many researchers have studied the outcrops of the Maikop in the KB and related it to the SCB (Popov et al., 1998; Hudson et al., 2008; Johnson et al., 2009; Efendiyeva et al., 2012). Although the Maikop deposits in the KB may serve as an analogue for those in the SCB, there are some differences of note between the deposits. Maikop deposits in the SCB are thought to represent classic black shale deposits (in which there is a large amount of unoxidized carbon deposited under deep-basin anoxic, reducing conditions), whereas the Maikop in the Kura Basin does not, being deposited in primarily oxic conditions with occasional suboxic/dysoxic development in discreet intervals (Johnson et al., 2009). Deposits in

the KB are also more proximal to the Caucasus Mountains, which may have been emergent during Maikop deposition, and the depositional environment was likely much shallower. Despite these differences, the primary stratigraphic correlations are thought to be consistent throughout the two basins (Johnson et al., 2009).

Chemostratigraphy

Redox-Sensitive Trace Metals

The elements V, U, Cr, P, Ba, Co, Mo, Ni, Cu, and Re are useful in identifying oxic to anoxic or euxinic paleodepositional environments. Anoxia develops in the absence of dissolved oxygen in the bottom waters of marine or lacustrine sedimentary basins. Anoxia develops as the rate of consumption of oxygen by organic matter (OM) consuming bacteria overtakes the influx of oxygen into the system. This can happen either as a result of intense OM degradation (consumption outpaces oxygen delivery to the system), or from limited input of oxygen to the system, commonly due to restriction of bottom-water circulation in restricted or isolated sedimentary basins (Tribovillard et al., 2006). Euxinic conditions, where hydrogen sulfide is resident in the water column, may or may not develop in anoxic conditions.

In anoxic waters, reducing conditions prevail that allow for the authigenic enrichment of trace metals. In order to use trace metals as paleo-anoxic indicators, it is important to distinguish authigenic input of elements versus detrital input. The fraction of authigenic element (X) may be calculated using the equation "detrital $X = (X/Al)_{\text{average shale}} \times Al_{\text{sample}}$," or by using statistical multivariate analyses (Jacot des Combes et al., 1999; Wijsman et al., 2001; Kryc et al., 2003; Tribovillard et al., 2006).

Authigenic enrichment of redox-sensitive trace metals is due in large part to the redox cycle of Mn and Fe (Tribovillard et al., 2006). Manganese occurs dominantly in seawater as Mn(II) and $MnCl^{+}$. In oxygenated waters, Mn(II) oxidizes to insoluble Mn(III) and Mn(IV) oxides (Calvert & Pedersen, 1993, 1996; Tribovillard et al., 2006). The Mn(IV) solid phases are referred to as Mn-oxyhydroxides. As the Mn-oxyhydroxides settle from the oxic zone to the sediment-water interface, trace metals adsorb onto the surface. In anoxic conditions (whether at the sediment-water interface or below), the oxyhydroxides are reductively dissolved and the trace metals are released, becoming available to be used in reactions involving the formation of new minerals like, for example, pyrite. Iron has a very similar redox cycle, and similarly transports redox-sensitive trace metals to anoxic zones for reductive capture into authigenic minerals (Tribovillard et al., 2006). Of the elements of interest mentioned earlier, V, Cr, Co, and Mo are primarily delivered to the sediment-water interface by this method.

Another driver of trace element enrichment in authigenic minerals under anoxic conditions involves the deposition of organic matter. The process of uranium enrichment is a good example. In oxygenated waters, uranium is stable as U(VI), which is complexed with carbonate ions in seawater to form $[UO_2(CO_3)_3]^{4-}$ (Languimer, 1978), which diffuses from the water column to the sediments through reduction and adsorption or precipitation as uranite into authigenic minerals (Barnes & Cochran, 1991; Klinkhammer and Palmer, 1991; Crusius et al., 1996; Morford & Emerson, 1999). Under anoxic, reducing conditions, removal of U into the sediment is accelerated by the formation of organometallic ligands in humic acids (Klinkhammer and Palmer, 1991; Zheng et al., 2002a; Zheng et al., 2002b; McManus et al., 2005; Tribovillard et al., 2006). Other elements that form organometallic ligands under reducing conditions are V,

Ni, and Cu, though the primary delivery of V to the sediment-water interface is through the redox-cycling of Mn.

Ni and Cu are primarily delivered to the sediments through the formation of organometallic complexes. Ni and Cu are released into pore waters as OM decomposes and is trapped in pyrite if sulfate-reducing conditions prevail (Huerta-Diaz and Morse, 1992; Fernex et al., 1992; Nameroff et al., 2002, 2004; Piper and Perkins, 2004; Algeo and Maynard, 2004; Tribovillard et al., 2006). Without the settling of organic sediments, even in reducing conditions Ni and Cu will not be enriched in the sediments. Enrichment in Ni and Cu therefore indicate high flux of organic matter and that reducing conditions were met, though good positive correlations between Ni-Cu enrichment and TOC have been shown regardless of the redox status (Tribovillard et al., 2006).

Organic Matter Type

Interpretation of the type and abundance of organic matter preserved in the sedimentary record is helpful in determining basin evolution via sedimentary source, factors that lead to organic matter preservation via anoxia or rapid sedimentation, and paleoclimate conditions. Pyrolysis was used as the primary method to determine the type of organic matter deposited in the samples of this study.

Organic matter is delivered to sediments as either dissolved organic carbon or particulate organic carbon (Hedges et al., 1997). In normal-marine environments, only about 10% of total OM produced leaves the euphotic zone (Tribovillard et al., 2006). Generally, the organic matter produced from terrestrial versus marine life may be characterized by differences in chemical

reactivity. This is evidenced primarily by increased degradability of most algal organic matter compared to terrestrial organic matter, or in the preservation of some algal groups over others in the fossil record (Goth et al., 1988; Arndt et al., 2013). Terrestrial organic matter is composed primarily of moderately to highly resistant biopolymers, such as cellulose, lignin, cutin, or cutan; this is a potential reason for higher resistance to degradation of terrestrial OM over marine OM. However, it is necessary to also consider that terrestrial OM will have undergone more extensive aging through soil burial, transport, and eventual delivery into marine environments. It has been suggested, therefore, that the lower degradability of terrestrial OM is due to protection by association with minerals or other organic matter (e.g. encapsulation; Huguet et al., 2008; Arndt et al., 2013).

Based on the differences in preservation potential between marine and terrestrial organic matter, abundances of either or both may be useful in resolving some of the interactions between paleo-productivity, sedimentation rate, and detrital input. For example, samples that are low in TOC (<1 wt%) that is dominant in type III (terrestrial) kerogens (as shown by pyrolysis), may represent an oxic depositional environment where either the production of marine organic matter is not sufficient to outpace the consumption of bottom-water oxygen, or the sedimentation rate is too low to bury the marine organic matter before degradation. Pairing organic matter type and abundance with geochemical indices of anoxia and detrital input provides greater resolution on the paleo-depositional conditions of the basin.

Re-Os Geochronology

Due to the unique aqueous chemistry of Re and Os, they were originally used as geochronometers for ore bodies in igneous and metamorphic rocks. In the past 20 years, Re-Os geochronology has been applied to organic-rich mudstones (ORM) using a method pioneered by Ravizza and Turekian (1989) and further developed by Ravizza et al. (1991), Cohen et al. (1999) and Creaser et al. (2002). The Re-Os geochronometer has been shown to be very reliable because of its geochemical stability and resistance to low-grade metamorphism, hydrocarbon maturation, and diagenetic alteration (Creaser et al., 2002; Rooney et al., 2010).

Most of the Re and Os found in ORMs have been found to be hydrogenous in origin (Cohen et al., 1999). Rhenium and Os in seawater is primarily sourced from continental runoff, with some areas receiving Re and Os through hydrothermal vents and extraterrestrial input. Rhenium and Os have a long residence time (750 Kyr and 20-50 Kyr, respectively) and both behave conservatively in the water column, so open ocean concentrations of Re and Os are thought to be generally homogenous (Colodner et al., 1993). However, inputs of Re and Os may vary from basin to basin depending on proximity to sources, variable source input, and restriction of circulation with open waters (McArthur et al., 2008; Cumming et al., 2012).

In addition to being used as a geochronometer, Re and Os abundances may be used as chemostratigraphic constraints. Rhenium may be used as an authigenic indicator because its detrital concentration is very low (Crusius et al., 1996). Rhenium and Os also tend to be more strongly fractionated in organic sediments of mixed terrigenous and marine origin with some O_2 remaining in the system, making the apparent fractionation of Re and Os a supporting indicator of organic matter type and oxic water conditions (Cumming et al., 2012; Harris et al., 2013). Due

to the homogenous nature of Os abundance in openly circulated marine water, $^{187}Os/^{188}Os$ may be used as a global chemostratigraphic marker, such as the $^{187}Os/^{188}Os$ excursion at the Eocene-Oligocene Transition (EOT; Dalai et al., 2006). However, caution must be applied in the use of such chemostratigraphic markers, as the composition of $^{187}Os/^{188}Os$ may be influenced by proximity to continental runoff, hydrothermal activity, or restriction of basin waters from open marine circulation. If the indications exist of close continental proximity, hydrothermal activity, or basin restriction, then the $^{187}Os/^{188}Os$ ratio is also useful as a paleoenvironmental indicator related to continental erosion and mid-ocean ridge magmatic activity (Sharma et al., 1999; Singh et al., 1999).

Methods

Sample Collection

Samples were collected from three primary sample sites: Perikeshkul, Mount Islamdag, and Shikhzahirli (Figure 1). Selection of sample sites was based on previous work where stratigraphic constraints drawn from microfaunal assemblages and chemostratigraphic data have already been developed (e.g. Popov et al., 2008; Hudson et al., 2008; Johnson et al., 2009). At each sample site, dark intervals of mudstone potentially rich in organic matter were identified and sampled (Figure 3).

Sampling was based primarily on meeting the needs of Re-Os geochronology. Rhenium and Os are captured into organic-rich mudstones during deposition at the sediment/water interface under limited oxygen conditions (Cohen et al., 1999; Colodner et al., 1993; Crusius et al., 1996; Ravizza and Turekian, 1992; Ravizza et al., 1991). The two primary mechanisms for

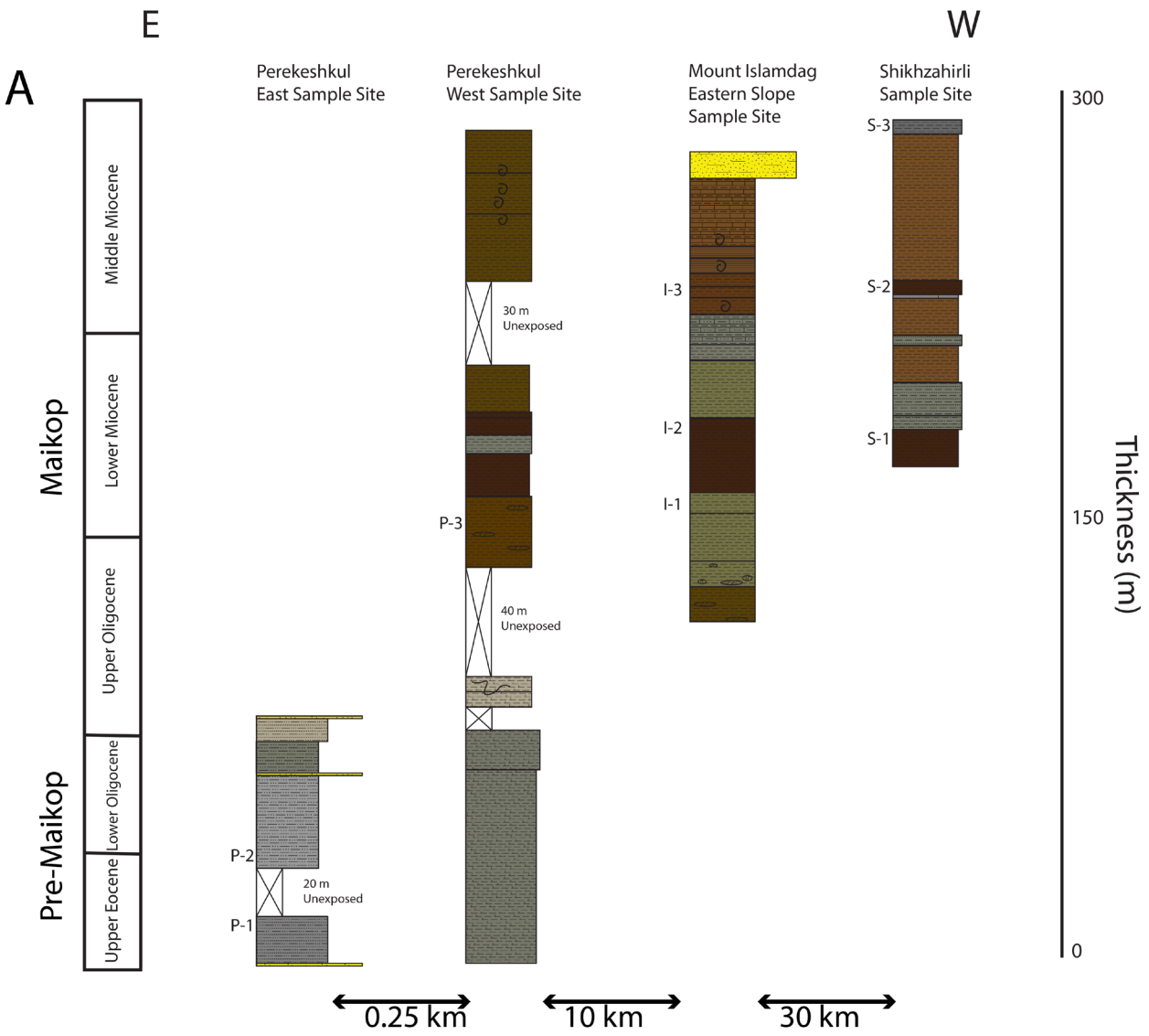

Figure 3 - Stratigraphic relationships shown between measured sections, spanning about 40 km laterally (See Figure 1). Designated sample locations within the stratigraphy (P-1, I-1, S-1, etc.) represent intervals where at least eight samples were taken for Re-Os analysis. Perikeshkul and Mount Islamdag measured sections are from Popov, (2008). Figure modified from Popov, (2008).

capture of Re and Os are reductive capture into sediments and adsorption onto organic matter, with the majority of the Re and Os becoming bound to organic matter (Cohen et al., 1999; Selby and Creaser, 2003; Yamashita et al., 2007; Georgiev et al., 2011; Rooney et al., 2012; Cumming et al., 2012). It has also been shown that some pre-existing Re and Os may be found in organic matter due to biogenic uptake during the lifespan of the organism (Rooney et al., 2016;

Racionero-Gomez et al., 2017). Post-depositionally, the Re-Os system is robust and remains stable through hydrocarbon maturation, and is even stable through contact metamorphism up to ~650˚ C (Creaser et al., 2002; Rooney et al., 2010). However, Re and Os are both chalcophilic and siderophilic, and due to the organic matter binding of Re and Os, they are very susceptible to alteration through oxidative weathering and hydrothermal activity (Rooney et al., 2012; Kendall et al., 2009; Georgiev et al., 2012). Therefore, great care was taken to avoid collecting samples with any evidence of these processes.

After identification of a potentially high organic horizon, a suite of samples was taken from that horizon. At least six samples are required to produce enough isotopic heterogeneity to produce an isochron, but in order to account for the potentially low sedimentation rates in the KB, eight samples were typically taken to ensure sufficient heterogeneity. Due to the relatively short residence time of Re and Os, isotope heterogeneity was achieved by sampling along a single lamina set, limiting vertical variation between samples to 5 cm or less. Samples with any signs of post-depositional alteration such as fractures, rust stains, calcite veins, and sulfur runoff were not collected for analysis. As it has been demonstrated that intense Re and Os weathering may occur up to 5 m in an outcrop due likely to oxidation of organic matter (Pierson-Wickmann et al., 2000; Georgeiv et al., 2012), samples were dug out of the outcrop sufficient to unearth fresh samples. In order to minimize individual sample heterogeneity, selected samples were typically about 50 to 100 g in size (Rooney et al., 2011). Two stratigraphic sections, one at Perikeshkul and the other at Shikhzahirli, were measured at sample locations where no previous section measurements had been published.

Sample Preparation

All sample powdering for bulk elemental, trace element, and pyrolysis analysis was conducted using rock crushing facilities at Brigham Young University. In order to ensure accurate analysis, rocks from each sample bag were selected based on size, with typical samples being 20-40 g in size (leaving larger sample sizes for Re-Os sample preparation). Selected samples were crushed into small chips using a steel hammer, then powdered in a tungsten-ball mill. In order to ensure maximum surface area exposure for pyrolysis, samples were sieved through a US No. 40 Standard Test Sieve (425 μm).

Pyrolysis

Pyrolysis analysis was completed at Brigham Young University using the Wildcat Technologies Hydrocarbon Analyzer with Kinetics (HAWK) pyrolysis and total organic carbon (TOC) instrument. Samples were expected to have less than 10% TOC, so 50-70 mg of powdered sample was placed into a crucible for analysis as recommended by the manufacturer. In order to obtain total organic and carbonate carbon, as well as source type and relative maturity, these samples were analyzed by whole-rock pyrolysis and total organic carbon/carbonate carbon (TOC+CC) techniques. A standard pyrolysis+TOC method was used, where the sample was heated from 300º C to 850º C at a rate of 25º C/minute during the pyrolysis stage, and from 300º C to 850º C at a rate of 25 ºC/minute during the oxidation stage (Espitalie and others, 1977; Peters and Cassa, 1994). Measurements include the amount of free hydrocarbons in the sample in mg HC/g rock (S1 Peak); kerogen yield, accomplished via the

amount of hydrocarbons generated through thermal cracking of non-volatile organic matter (S2 Peak); organic carbon dioxide yield, which is the amount of CO2 in mg CO_2/g rock produced during pyrolysis of kerogen (S3 Peak); mg carbon/g rock produced from organic residue remaining after pyrolysis of kerogen is completed (S4 Peak); Tmax, which is the temperature at which the maximum generation of hydrocarbons from cracking of kerogen occurred during pyrolysis (measured at the top of the S2 peak); total organic carbon (TOC) in weight %; and carbonate carbon (CC) in weight %. From these measurements, interpretative calculations are made including the adsorption index, oil saturation index, hydrogen index, oxygen index, production index, generative organic carbon (weight %), and non-generative organic carbon (weight %). It is important to note that due to the mineral matrix effect, which refers to the interference of clay minerals with the release of hydrocarbons, pyrolysis results for samples of low (<0.5 wt %) may be considered more qualitative than quantitatively accurate (Peters, 1986).

X-Ray Fluorescence (XRF)

XRF analysis was performed using the Rigaku ZSX Primus II at Brigham Young University. For trace element analysis, samples were pressed into discs by combining 8.3 g of sample with 1.132 g of SpectroBlend 44 μm powder (composed of 81% C, 13.5% H, 2.9% O, and 2.6% N, with 0-10 ppm impurities of Ag, As, B, Cd, Hg, Pb, and Sn). The sample mixtures were pressed to 50,000 lbs of pressure using tungsten pressing discs in a pressing assembly. For bulk element analysis, fused disc samples were prepared by combining 1.23 g of sample with 8.61 g of lithium borate flux, then fused using a platinum crucible in a Katanax K1 fused disc preparation machine. In order to ensure proper machine operation, samples were analyzed along

with standards JA-1 (andesite from Japan), JA-2 (andesite from Japan), SGR-1 (mudstone from the Green River Formation), JB-1A (basalt from Japan), JR-1 (rhyolite from Japan), and RGM-1 (rhyolite from Glass Mountain). Major and minor elements analyzed via XRF include Si, Ti, Al, Fe, Mn, Mg, Ca, Na, K, P, Ba, Ce, Cr, Cu, Ga, La, Nb, Nd, Ni, Pb, Rb, Sc, Sm, Sr, Th, U, V, Y, Zn, and Zr.

Leco Sulfur Analysis

Sulfur analysis was conducted using a Leco Furnace Sulfur Analyzer at the ALS Canada geochemistry lab in British Columbia. 0.01 to 0.1 g of each sample was heated in the Leco furnace to approximately 1350˚ C in an induction furnace while passing a stream of oxygen through the sample. Sulfur dioxide released from the sample was measured by an infrared (IR) detection system to measure the total sulfur released from the sample.

Inductively Coupled Plasma Optical Emission Spectrometry (ICP-OES)

In order for samples to be accurately analyzed in the ICP-OES, they first had to be homogeneously dissolved into solution. Fusion of samples into glass discs with lithium borate flux breaks down mineral structures to form a mechanically strong glass that may either be dissolved in acid without the use of HF, whole or powdered, so samples were prepared for acid digestion by powdering the fused discs used in XRF analysis (see Igamells, 1970). As aluminum had been analyzed in the XRF, the discs were powdered in an alumina-ceramic shatterbox in order to avoid contamination with elements not yet analyzed (specifically Co, which tungsten

shatterboxes are contaminated with). Powdered discs were dissolved in an acid solution containing 0.7 g of sample, 20 g of 10% HCl solution, 10 drops of 10M HNO_3, and approximately 30 g of milli-Q water to a total volume of 50 mL (~50g). Samples were then analyzed using a ThermoScientific iCAP 7400 ICP-OES in the labs of Brigham Young University. Standards run along with samples were JA-2 and SGR-1, which were prepared for ICP-OES using the same process. Crossover data between the XRF and ICP-OES was compared and determined to be within a few percent error. Elements analyzed via ICP-OES include Mo, Co, and As. Other elements resulting from ICP-OES analysis were used to verify the measurements performed via XRF, including for Ba, Cr, Cu, Ni, Sr, V, and Zn.

Re-Os Analysis

As Re and Os are associated with the deposition of organic matter and a relationship is often shown between Re and Mo, samples to be analyzed for Re-Os geochronology were selected based on TOC values, the abundance of molybdenum and current stratigraphic constraints. In order to minimize sample contamination, selected samples were polished using silica carbide grit pads to remove surfaces potentially exposed to surface weathering and that may have contaminated by metal tools. Samples were then broken into pieces in a ceramic mortar and pestle and powdered in an alumina-ceramic shatterbox to yield 30-80 g of powdered sample.

The detrital component of Os in organic-rich mudstones causes an increase in geologic scatter around the isochron. In order to minimize this scatter and increase the accuracy of the Re-Os geochronometer, a digestion method that limits the removal of any detrital Re and Os

component must be employed. The acid digestion method used in this study are detailed in Selby and Creaser (2003). In this method, whole-rock powders are reacted with a Re-Os purified digestion medium of CrO_3 in 4 N H_2SO_4 (0.2 g CrO_3 per ml of 4 N H_2SO_4). Approximately 1 g of each sample with less than or greater than 5% TOC was digested in 8 mL or 16 mL of CrO_3-H_2SO_4 solution, respectively, together with a mixed tracer solution of ^{185}Re and ^{190}Os in a sealed Carius tube at 240˚ C for 48 hours. Following acid digestion, Os isolated from the solution using $CHCl_3$ solvent extraction and micro-distillation. Following the Os extraction from the Cr-H_2SO_4 solution Re is isolated and purified using NaOH-Acetone solution extraction and anion chromatography.

Due to the high ionization potential of Re and Os (~9eV, Dickin, 2008), samples were analyzed using negative thermal ionization mass spectrometry (NTIMS) in a Thermo Scientific Triton TIMS instrument. Analysis via N-TIMS allows measurement of Re and Os at the nanogram to subnanogram concentration, respectively, with accuracy up to ±0.5% 2σ (Volkening et al., 1991; Creaser et al., 1991). The purified fractions of Re and Os were loaded on to Ni and Pt wire filaments, with the Re isotope compositions determined via static Faraday collection, and the Os isotope compositions obtained via peak hoping using a secondary electron multiplier. For the $Cr^{VI}O_3$–H_2SO_4 solution total procedural blanks during this study were 18.0 ± 3.0 pg and 0.20 ± 0.05 pg (1 S.D., n = 4) for Re and Os, respectively, with an average $^{187}Os/^{188}Os$ value of 0.17 ± 0.05 (n = 4).

Statistical Analysis

Bulk geochemical data were analyzed statistically to produce clustering of samples and geochemical element abundances using JMP Pro 13 software. In JMP, statistical hierarchal

$$D_{KL} = \frac{\left\|\overline{x_K} - \overline{x_L}\right\|^2}{\frac{1}{N_K} + \frac{1}{N_L}}$$

clustering was achieved through the calculation of Cubic Clustering Criterion (CCC). Calculating CCC involves plotting sample results on a hypercube containing a uniform distribution of reference points, then using a heuristic formula to estimate the error of a distance (between reference points and actual points) based clustering algorithm in the reference distribution. For this study, Ward's method was used, where distance is calculated as:
Where C_K is the Kth cluster, x_K is the mean vector for cluster C_K, and N_K is the number of observations in C_K. A high value of CCC corresponds to smaller error (as calculated by R^2); therefore, the higher the CCC the more reliable the clusters. Using the CCC, a number of clusters are chosen that are statistically and geologically reasonable. Samples are divided into seven clusters with a CCC of 18.47, which was the highest value of CCC calculated between varying numbers of clusters.

Clusters were then plotted on a dendrogram to display their relative relationships to each other. Line distances in the dendrogram correspond to distances between clusters, and therefore display the mathematical similarity between geochemical signatures. The dendrogram was also plotted with two-way clustering so as to show element relationships, and a heat map was plotted to visually represent the element clustering between samples. Using the dendrogram, improved

correlations between geologic units in measured sections of the Maikop in Eastern Azerbaijan were drawn.

Results

In this section, results from pyrolysis, elemental analysis, and Re-Os geochronology from each sample suite are compared. Nine sample suites were taken that consist of eight samples each from the same lithologic unit. Three sample suites were taken from Perikeshkul, three from Mount Islamdag, and three from Shikhzahirli. Sample suites were taken from older, non-Maikopian rocks at Perikeshkul (Figure 3) in order to establish geochemical continuity throughout the stratigraphic section and to analyze for possible Os excursion during the Late Eocene (Dalai et al., 2006; Peuker-Ehrenbrink & Ravizza, 2012). Moving from east to west, samples were taken from Perikeshkul (suites designated P-1 through P-3, stratigraphically oldest to youngest), Mount Islamdag (I-1 through I-3, oldest to youngest), and Shikhzahirli (S-1 through S-3, oldest to youngest), covering a lateral distance of about ~40 km, with the Peikeshkul and Islamdag sample sites only 10 km apart (Figure 3).

Organic Matter Preservation and Type

TOC in Maikop samples of the Kura Basin is generally low (~1% TOC average), with the exception of samples taken from Islamdag (~3% TOC average). Hydrogen Index (HI) values are lowest in samples from the youngest Islamdag (S-3) sample suite (~30 mgHC/gTOC) and Perikeshkul P-1 and P-2 (~10 mgHC/gTOC; see Figure 4). Hydrogen indices from Shikhzahirli are higher (150-200 mgHC/gTOC), with the Islamdag I-1 and I-2 sample suites show the highest

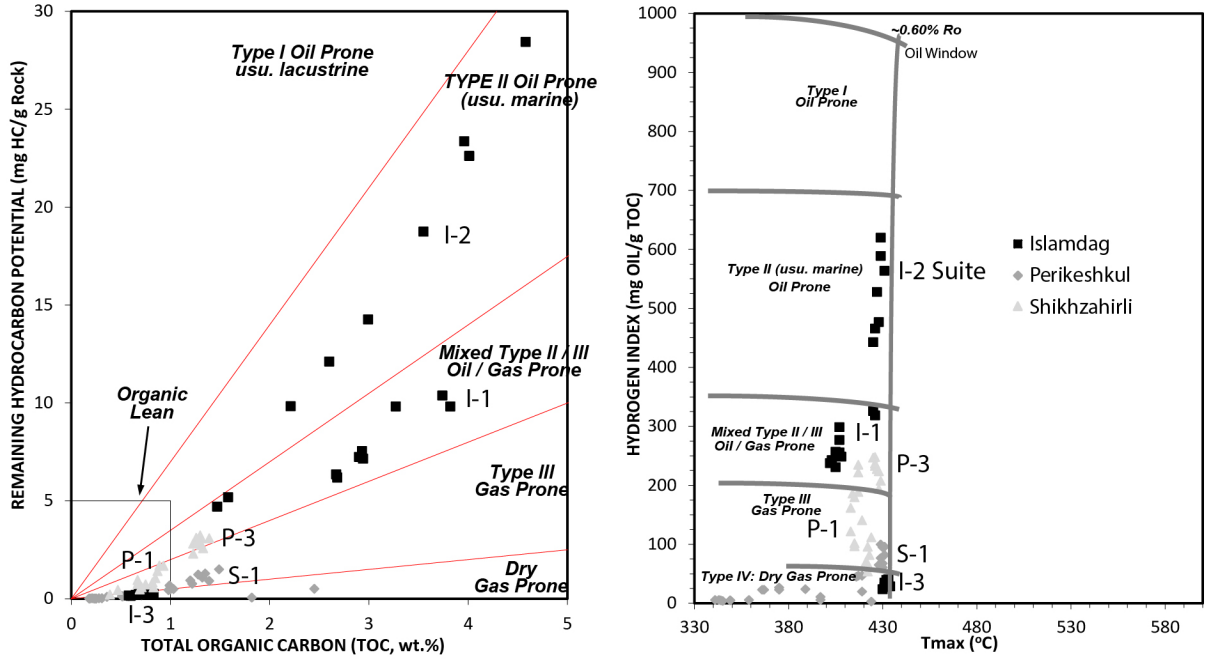

Figure 4 - (Left) Total organic carbon (TOC) and remaining hydrocarbon potential based on results from HAWK pyrolysis. Sample suites (8 samples each) are marked near their clusters (see Figure 3). (Right) Maturity of hydrocarbons in samples based on Hydrogen Index vs. Tmax from HAWK pyrolysis.

HI values (~400 mgHC/gTOC). Oxygen Index (OI) values are consistently inversely proportional to HI values for all sample suites. S2 peaks (kerogen yield, or the remaining hydrocarbon potential in the samples) were highest in the lower two Islamdag sample suites (I-1 and I-2), with average values of 8 and 15.5, respectively. All other sample suites had a kerogen yield of 0.2 to 3. Comparisons utilizing TOC, HI, and S2 reveal much of the preserved TOC is terrigenous in nature, with kerogen types being dominantly type III and type IV, although low Tmax values suggest that some kerogens may have undergone minor thermal cracking into the oil window. Deviations from this general behavior are seen in the lower two suites from Islamdag (I-1 and I-3) and the P-3 sample suite from the western Perikeshkul site, which display mixing of type II/III kerogen and, in the case of the middle Islamdag sample suite, a predominantly marine source (type II) kerogen.

Utilization of organic paleo-proxy elements Cu and Ni compared with TOC reveals a good correlation, indicating that significant post-depositional organic matter degradation did not take place below the sediment-water interface (Figure 5). Thus, the correlation supports the low Tmax values that indicate immature organic material. Hydrocarbon maturation and migration has not likely taken place in these samples; therefore, TOC measurements probably reflect the original depositional organic matter content of the samples, as no hydrocarbon maturation and migration is indicated. However, these indicators do not provide clues as to the paleo-productivity of the area, as organic matter may have degraded in the water column or at the sediment-water interface, thereby preventing the authigenic enrichment of Cu and Ni captured in organic matter in the water column.

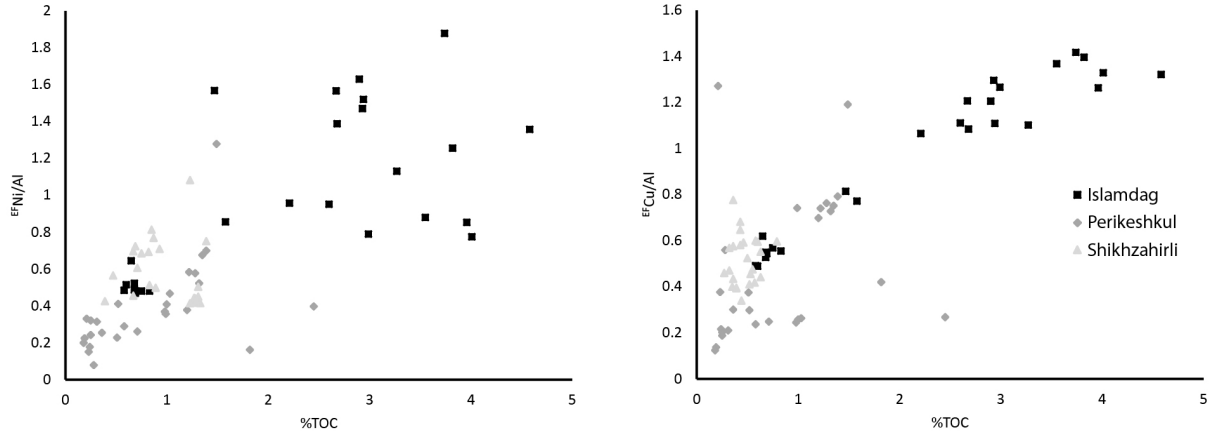

Figure 5 - Copper and Ni may be used as indicators for the preservation or degradation of organic matter in a sample because they are primarily enriched in authigenic minerals through the formation of organometallic complexes (see text for explanation). A strong trend in Cu and Ni to TOC may indicate that significant organic matter degredation has not taken place below the sediment-water interface.

Detrital Input

Primary detrital indicators in these samples include Ti, Al, Ga, La, and Sc, as these elements are typically bound in continental minerals that are resistant to degradation (Kryc et al.,

2003; Tribovillard et al., 2006; Wood and Samson, 2006). Good correlations are observed between each of these elements, indicating a small fraction of authigenic enrichment of these elements (). Overall, the samples collected as part of this study are depleted in detrital elements, with a few exceptions. Enrichment factors calculated from average black shale composition (Wedepohl, 1971, 1991) reveal that the P-1, I-2, S-1, S-2, and S-3 sample suites are depleted in Ti, with Al enrichment ranging from 0.60 to 1.20. Enrichment of both Ti and Al appears most significantly in the P-3, I-1, and I-3 sample suites, which displayed average enrichment factors of Ti and Al of ranging from 1.00 – 1.20 and 1.20 – 1.60. Ga, La, and Sc are typically bound in minerals with low solubility (e.g. bauxite) and correlate well with Ti and Al in these samples, so they are used to support the interpretations of detrital influx (Wood & Samson, 2006). Similar values of enrichment are observed in sample suites, with enrichment of La, Ga and Sc in the I-3 and P-3 sample suites at 1.0, 1.40 and 1.60, respectively. The only significant deviation from enrichment behavior between Ti, Al, and Sc exists in the Perikeshkul sample suite P-2, which previous studies suggest is pre-Maikopian in age (Hudson et al., 2008), which is anomalously enriched in Sc (EF of 1.5).

Anoxic Indicators

Elemental indicators for anoxia include U, Th, Mo, V, Cr, Ni, and Cu. Abundances of these elements were plotted on bivariate diagrams using elements and element ratios (Figure 7). All sample suites except one showed enrichment factors of Mo below 20, U/Th ratios below 0.75, V/Cr ratios below 2.00, and had generally low values of TOC (~1 wt % average TOC). The values of these ratios and the enrichment factor of Mo suggest that all of these samples were

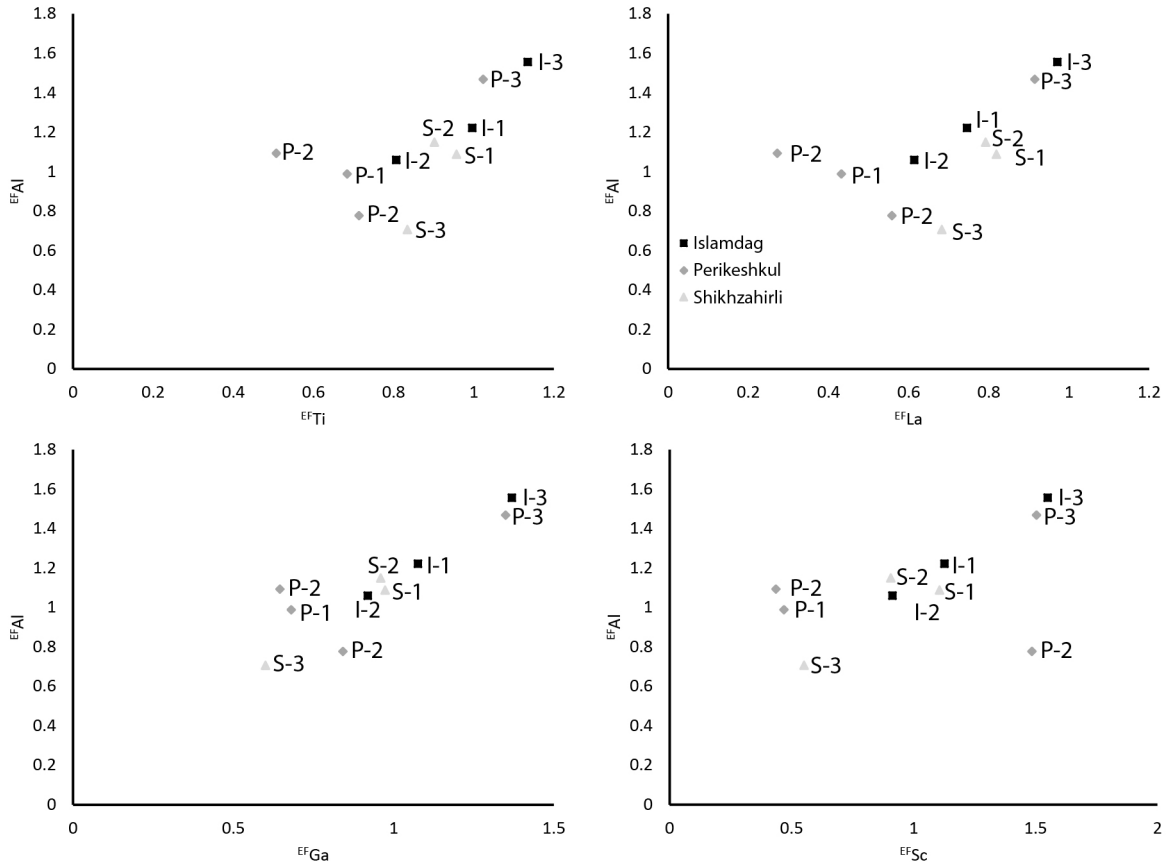

Figure 6 - Enrichment factors of elements typically bound in insoluble, resistant detrital minerals that may be used as a proxy for relative detrital input. Comparison of plots reveals a consistent detrital indication, bolstering the reliability of these proxies by ruling out post-depositional authigenic enrichment. Variation of enrichment between elements indicates deviance of abundances of typical detrital minerals from average deposits of black shale.

deposited in oxic conditions (Jones & Manning, 1994). When comparing values of TOC with Al-normalized enrichment factors of Cu, Ni, U, Va, and Mo, no correlation is observed, indicating deposition of sediment in oxic conditions (Tribovillard et al., 2006). The only sample suite to deviate from this behavior is the Islamdag S-1 sample suite, which has average ^{EF}Mo above 50, U/Th values above 1.25, V/Cr values between 2.00 and 4.25, and average TOC of 4 wt %. These values indicate that this sample suite was deposited in suboxic to anoxic conditions (Jones & Manning, 1994). Comparisons of TOC with enrichment factors of Al-normalized Cu, U, and Mo show a weak overall correlation, but a significantly higher relative enrichment. These results similarly indicate that the S-1 sample suite was deposited in suboxic to anoxic conditions. The

results of organic preservation throughout the sample suites presented in this study are similar to those found by previous studies (Hudson et al., 2008; Johnson et al., 2009).

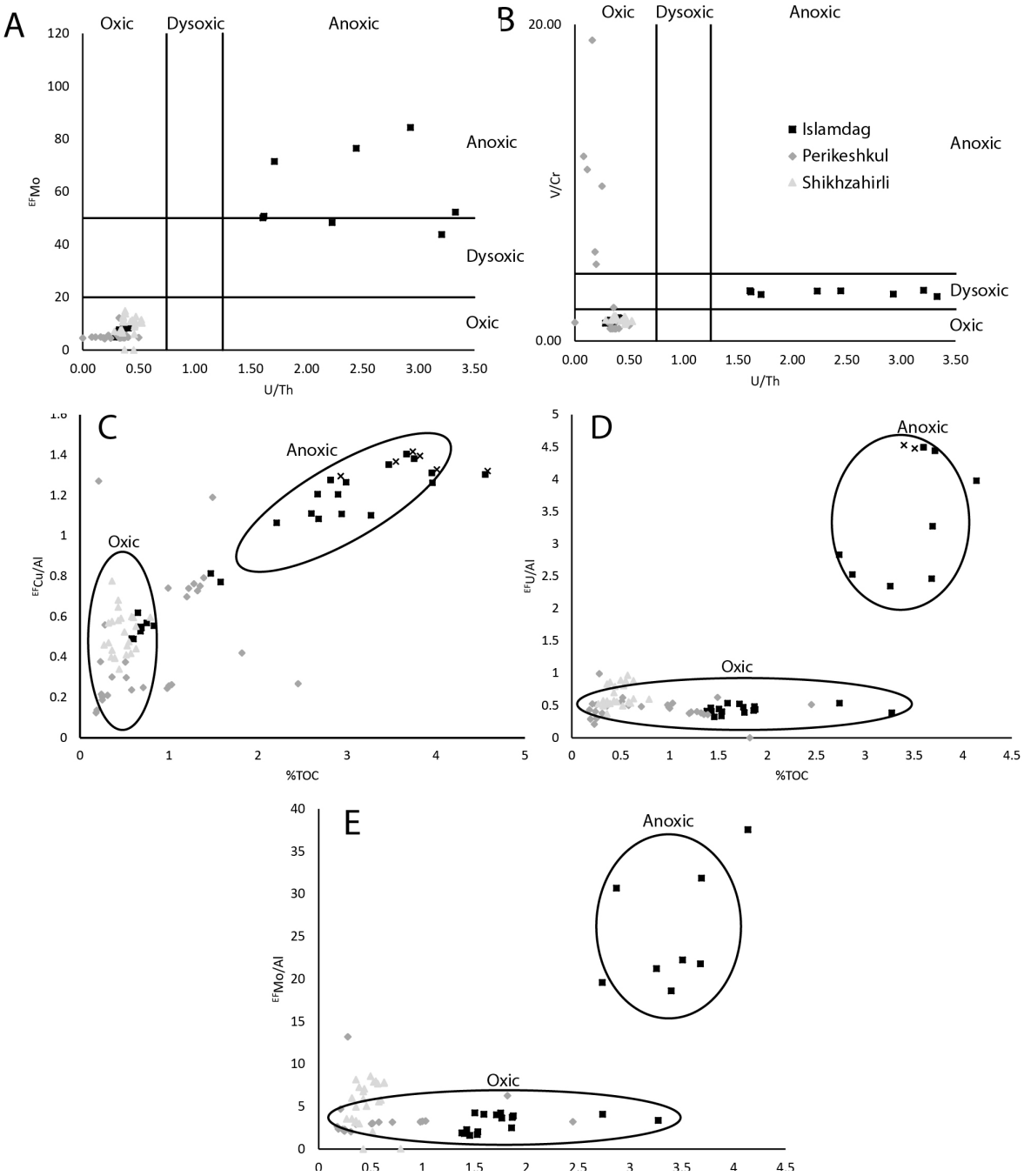

Figure 7 - Oxic and anoxic geochemical indicators. (A) and (B) are quantitative anoxia indicators from Jones & Manning (1994). (C), (D) and (E) are qualititative geochemical indicators of anoxia from Tribovillard et al. (2006). With small variations, most geochemical indicators agree that all of the Maikop samples collected from the Kura Basin were deposited in oxic bottom water conditions save for the I-1 sample suite from Islamdag, which consistently plots in anoxic to dysoxic bottom water conditions.

Re-Os Geochronology

Of the five sample suites analyzed for Re-Os geochronology, only one Re-Os data set successfully produced a meaningful age and uncertainty: the Islamdag I-3 sample suite. Collectively the Re-Os data for the Islamdag I-3 possess $^{187}Re/^{188}Os$ and $^{187}Os/^{188}Os$ values of ~2000-6000 and ~1.0 and 2.3, respectively that are positively correlated. The entire sample set yield a Re-Os date of 17.2 ± 3.2 Ma, with an initial $^{187}Os/^{188}Os$ of 0.71 ± 0.23. However, significant scatter is exhibited by the data set about the best-fit line as described by the exceptionally high mean square of weighted deviates (MSWD) value of 660. The scatter could be the result of post-depositional disturbance to the Re-Os systematic, and/or variability in the initial $^{187}Os/^{188}Os$ composition of the sample set. Calculated at 17.2 Myrs the sample set describe two subsets that yield initial $^{187}Os/^{188}Os$ values of ~0.80 and ~0.60, which coincide with the same samples that fall above and below the best-fit line of the complete data set (Figure 8). The two subsets yield Re-Os dates of 16.9 ± 2.2 Ma (initial $^{187}Os/^{188}Os$ = 0.80 ± 0.14, MSWD = 33) and 18.3 ± 1.7 Ma (initial $^{187}Os/^{188}Os$ = 0.56 ± 0.13, MSWD = 21). Both date determinations are identical within uncertainty. Samples that fall above and below the best-fit line of the complete data set do not group into separate conformable ages of strata, respectively. The lack of stratigraphic grouping of variable initial Os indicates that the variation in initial Os cannot be due to a single change in depositional conditions, nor does the variation between samples have cyclic variation going up the stratigraphic column.

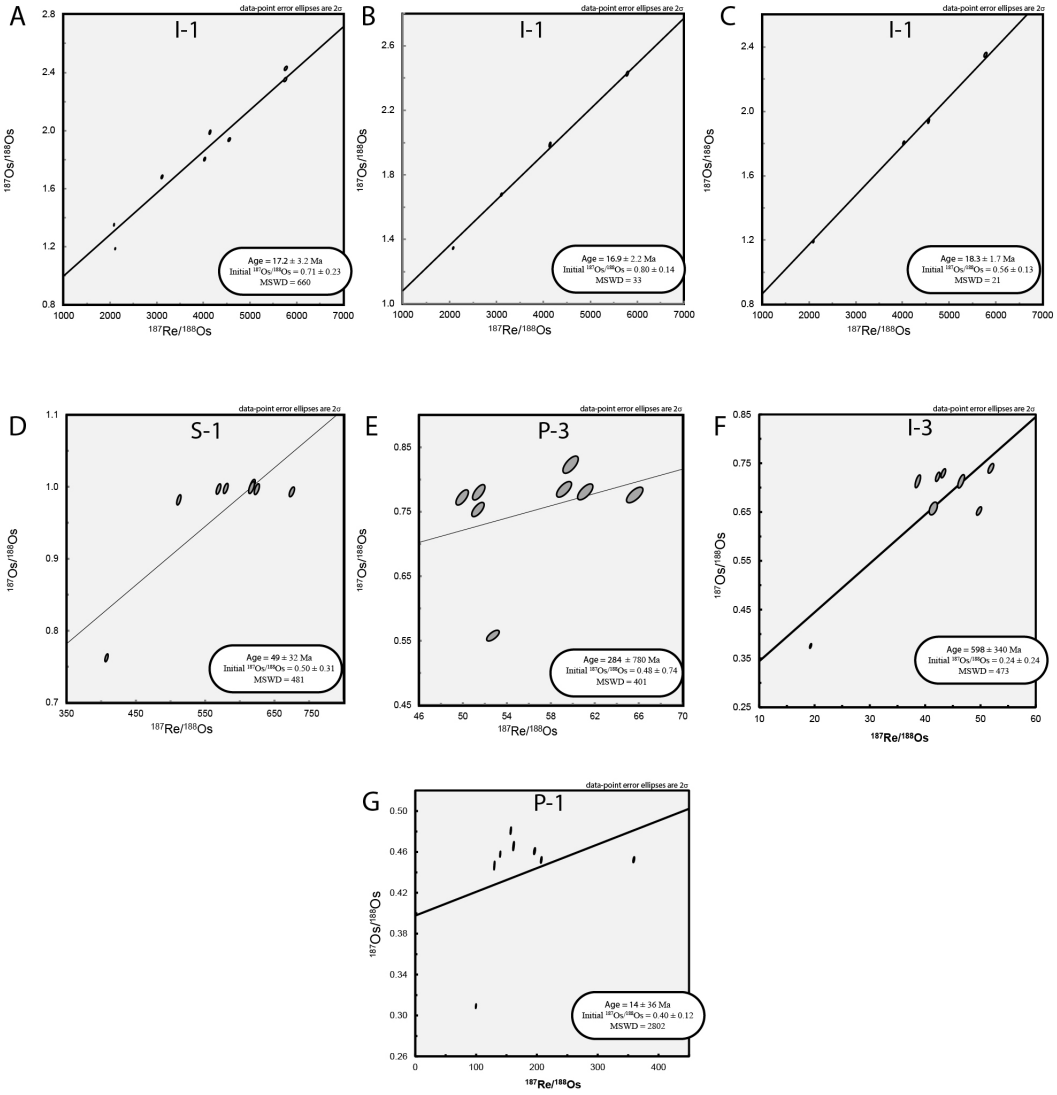

Figure 8 - 187Re/188Os vs 187Os/188Os plots. The Re-Os data from the I-3 sample suite yielded the only meaningful age determinations (A)(B)(C). (A) displays the solution using the full sample suite from I-3. Using the full suite the best-fit of the data shows considerable scatter (see text for discussion). However, the distribution above and below the isochron led to the splitting the I-3 sample suite in to two sub groups (B)(C). The two sub groups yield a Re-Os date within uncertainty (B, C). (D)(E)(F)(G)187Re/188Os vs 187Os/188Os plots for the sample suites studied for Re-Os geochronology. These four sample suites failed to produce statistically meaningful Re-Os isochrons.

Stratigraphic Correlations

Hierarchal clustering statistics confirmed that samples in a suite represented one lithologic unit, as all samples in each respective suite was found to be nearly geochemically

identical. Furthermore, relationships between the geochemistry of sample suites was quantified by hierarchal clustering analysis and represented on a hierarchal diagram on which the geometric appearance of the diagram is mathematically determined (Figure 9). Previous work (Hudson et al., 2008; Johnson et al., 2009) suggests that the three sample localities are time correlative, and geochemical comparison of sample suites from this study reinforce this. Bulk geochemical analysis indicates a strong relationship between the upper Islamdag (I-3) and upper Perikeshkul (P-3) sample suites (Figure 9). A similarly strong relationship exists between the S-1 and S-2 sample suites of Shikhzahirli, which in turn are shown to have a moderately strong relationship to the I-3 and P-3 sample suites. The P-2 and S-3 sample suites show a moderate relationship that is likely related to similarities in mineralogy and depositional conditions, as they are very unlikely to be related stratigraphically. The other sample suites, including the P-1 and I-2 suites, are weakly related to the other sample suites, indicating very different depositional conditions and sediment supply.

Discussion

The results of this study indicate that, despite its ability to generate large volumes of oil and gas, the majority of the Miocene Maikop found in outcrop in the KB of eastern Azerbaijan may not be considered to have been deposited in a marine anoxic setting, in agreement with the conclusions of Hudson et al. (2008) and Jonson et al. (2009). The majority of the Miocene Maikop preserved in the KB is generally low in TOC (~1%) that is primarily sourced from terrigenous input. Only the Islamdag lower and middle sample suites had significant TOC values (up to 5%), which samples were from the lower and middle Islamdag sample suites. Geochemical analysis indicated that the lower Islamdag sample suite was of mixed terrigenous

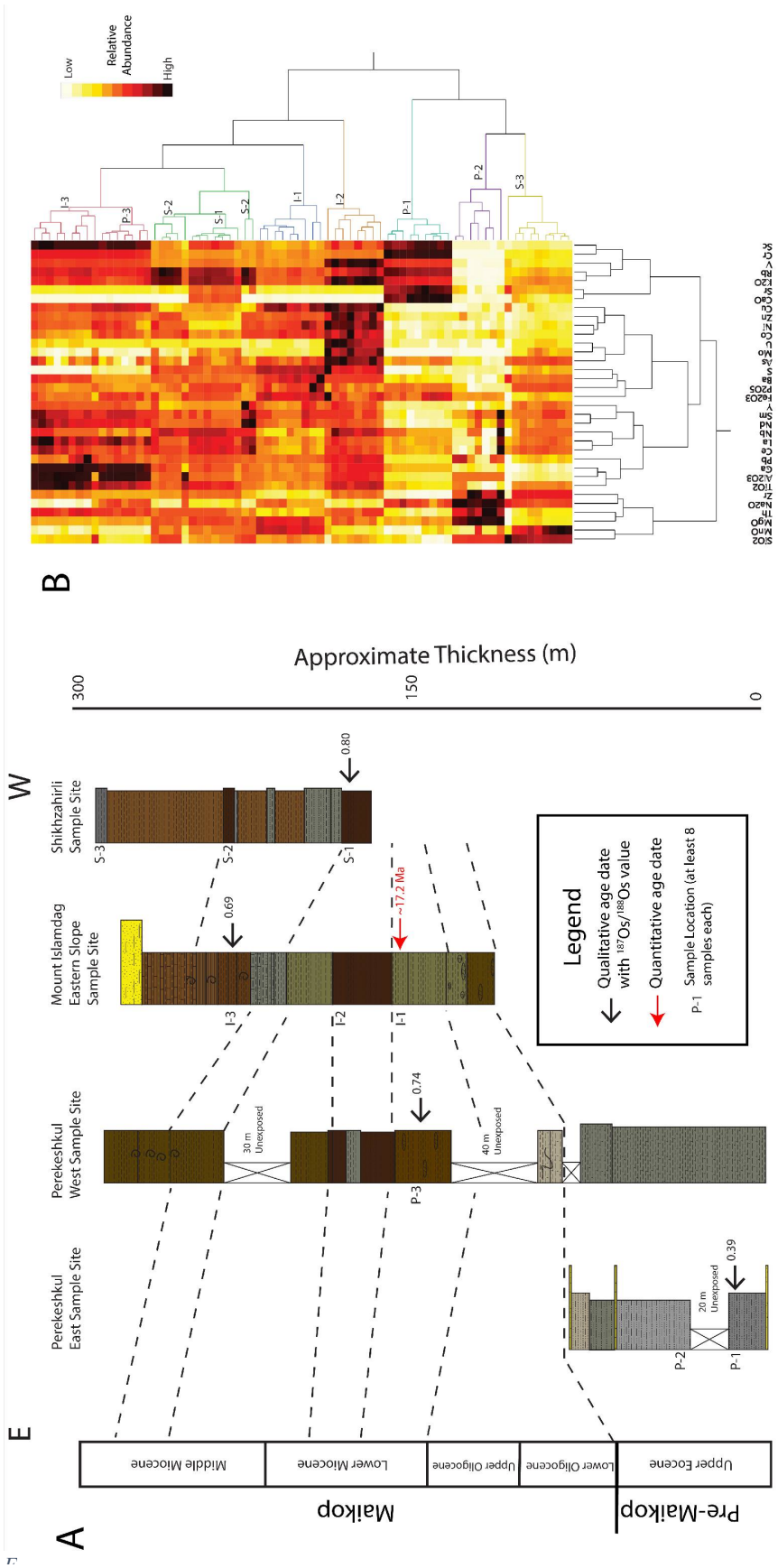

Figure 9 - (A) Stratigraphic correlations of sample site measured sections, modified from Popov et al. (2008). Five sample suites were measured for Re-Os geochronology. Of the five, one (I-1) produced an isochron date of ~17.2 Ma. The other four are dated qualitatively using the global seawater curve for $^{187}Os/^{188}Os$ compiled by Peuker-Ehrenbrink & Ravizza (2012; see Figure 10). Each sample suite location refers to eight samples taken from a single lithologic unit. Stratigraphic correlations are based on microfaunal assemblages (Popov et al., 2008), geochemical statistical clustering analysis, and Re-Os geochronology. (B) Geochemcal two-way cluster analysis displaying statistically determined relationships between sample suites and the elements analyzed for each sample. Clustering was determined using cubic clustering criterion (see Equation 1).

and marine organic matter, the preservation of which was likely due largely to suboxic to anoxic conditions in the bottom waters of the basin. Although the middle Islamdag suite had similar values for TOC, geochemical analysis indicated dominant marine organic matter preservation in oxic conditions, indicating that preservation of organic matter was likely due either to high productivity rates of organic matter outpacing organic matter degradation at the sediment-water interface, a high sedimentation rate, or a combination of both.

Re-Os geochronology, though only successful for one of the five sample suites, provides important new data in the South Caspian and Kura Basins. An age date of ~17.2 Ma for the lower Islamdag sample suite provides a datum of reference for the extensive bio-, chemo-, chrono-, and lithostratigraphic data that has been collected throughout the Kura Basin and possibly the SCB. However, there are two puzzling aspects of the lower Islamdag isochron. The first is the production of two isochrons of identical date, but differing initial $^{187}Os/^{188}Os$ compositions. The reason for the split is unknown, as there are apparently no other elements analyzed in this study that show the same separation pattern between samples. It may be possible that the differences are the result of rapid, dynamic changes within the hydrodynamics of the basin at the time of deposition. These rapid changes may be the result of increases and decreases in restriction in the SCB caused by tectonics, relative sea level change, or a combination of the two. Additionally, the lower value for initial $^{187}Os/^{188}Os$ of 0.56 suggests that sediment being sourced to the basin is less radiogenic, indicating significant volcanic sediment source. Therefore, a significant sediment source at this time was likely coming from the mafic volcanic Talysh Mountains to the south, as volcanic sediments tend to contain less radiogenic $^{187}Os/^{188}Os$ compositions. The second puzzling feature of the Re-Os data from the lower Islamdag suite is the high enrichment in common Os and Re, as represented by ^{192}Os (sample suite I-1; Table 2).

This could be due to more efficient uptake of Os into organic matter, a higher preservation of organic matter past the sediment-water interface that allowed for more authigenic enrichment of Os, an increased supply in Os due to oxidative weathering of Os-rich minerals on the continent, or a combination of any of these factors (Ravizza and Esser, 1993; Selby and Creaser, 2003; Baioumy et al., 2011; Cumming et al., 2012).

The failure of the other sample suites to produce an isochron is due to the lack of heterogeneity in the $^{187}Re/^{188}Os$ vs $^{187}Os/^{188}Os$ compositions between collected samples. The exact methods of obtaining heterogeneity of Re ad Os between samples are not yet fully understood (Ravizza and Turekian, 1989; Creaser et al., 2002; Georgiev et al., 2012; Cumming et al., 2012; Harris et al., 2013). Lack of heterogeneity may have come about through disturbance of the Re-Os system through oxidative weathering, through differences in Re and Os uptake between sample sites due to variations in water-column chemistry or organic matter type, sedimentation dynamics or due to insufficient spacing of sampling, vertically or horizontally. As the potential for oxidative weathering in outcrop samples cannot be completely ruled out, future studies should seek to obtain Re-Os isochrons from core samples.

Despite the lack of successfully produced isochrons, it is still possible to derive some depositional control from the initial $^{187}Os/^{188}Os$ ratios. Osmium isotope ratios for sample suites provide qualitative control on either basin dynamics or deposition age based on correlation (or lack thereof) with the global seawater $^{187}Os/^{188}Os$ curve and verified by comparison to the isochron age date obtained from the I-1 sample suite (; Peuker-Ehrenbrink and Ravizza, 2012). For example, the I-1 suite (dated at ~17.2 Ma) has an initial $^{187}Os/^{188}Os$ ratio of 0.71. On the global sea level curve, the time period that corresponds to $^{187}Os/^{188}Os$ values that range from 0.7 to 0.8 is from the late Middle Oligocene through the Middle Miocene, a qualitative age

constraint that coincides with the age produced via isochron. Furthermore, the correlation of initial $^{187}Os/^{188}Os$ values with the global sea level curve indicates that, despite the indications of bottom water dysoxia/anoxia, the Kura Basin was likely still circulating with the open ocean enough to produce a similar $^{187}Os/^{188}Os$ value. This reinforces geochemical data from this study and others that suggest limited circulation, but not complete basin isolation during the Oligocene-Miocene (Hudson et al., 2008).

The initial $^{187}Os/^{188}Os$ values for the P-3, S-1, and I-3 sample suites are 0.74 ± 0.004, 0.80 ± 0.05, and 0.69 ± 0.003, respectively, with initial values calculated between 12 and 22 Ma. These values correspond with the global $^{187}Os/^{188}Os$ curve from the late Middle Oligocene through the late Middle Miocene (Figures 9 and 10). Sample suite P-3 is interpreted to be of similar age to sample suite I-1, which is reinforced by their nearly identical $^{187}Os/^{188}Os$ ratios. Suite S-1 overlies sample suite I-2 and I-1, and is interpreted to be Middle Miocene in age. The stratigraphically uppermost sample suite tested for Re and Os is suite I-3, which is interpreted to be late Middle Miocene in age. All of these sample suites correlate well with the global $^{187}Os/^{188}Os$ curve, indicating limited basin restriction during these times to allow for enough circulation with the open ocean to homogenize Re and Os concentrations.

Samples from the P-1 sample suite are considered to be the oldest, and are interpreted to be pre-Maikopian rocks that were deposited near the Eocene-Oligocene transition (Hudson et al., 2008). The P-1 sample suite has an average initial $^{187}Os/^{188}Os$ ratio of 0.34 ± 0.15, which initial value was calculated assuming an age of 39 to 29 Ma. This low $^{187}Os/^{188}Os$ value correlates to the osmium isotope excursion at Eocene-Oligocene Transition (EOT), as discussed by Dalai et al (2006) and reflected in the global $^{187}Os/^{188}Os$ sea level curve (Figure 10). The presence of the

excursion in these samples also indicates that the basin was connected to open marine waters during deposition of this interval.

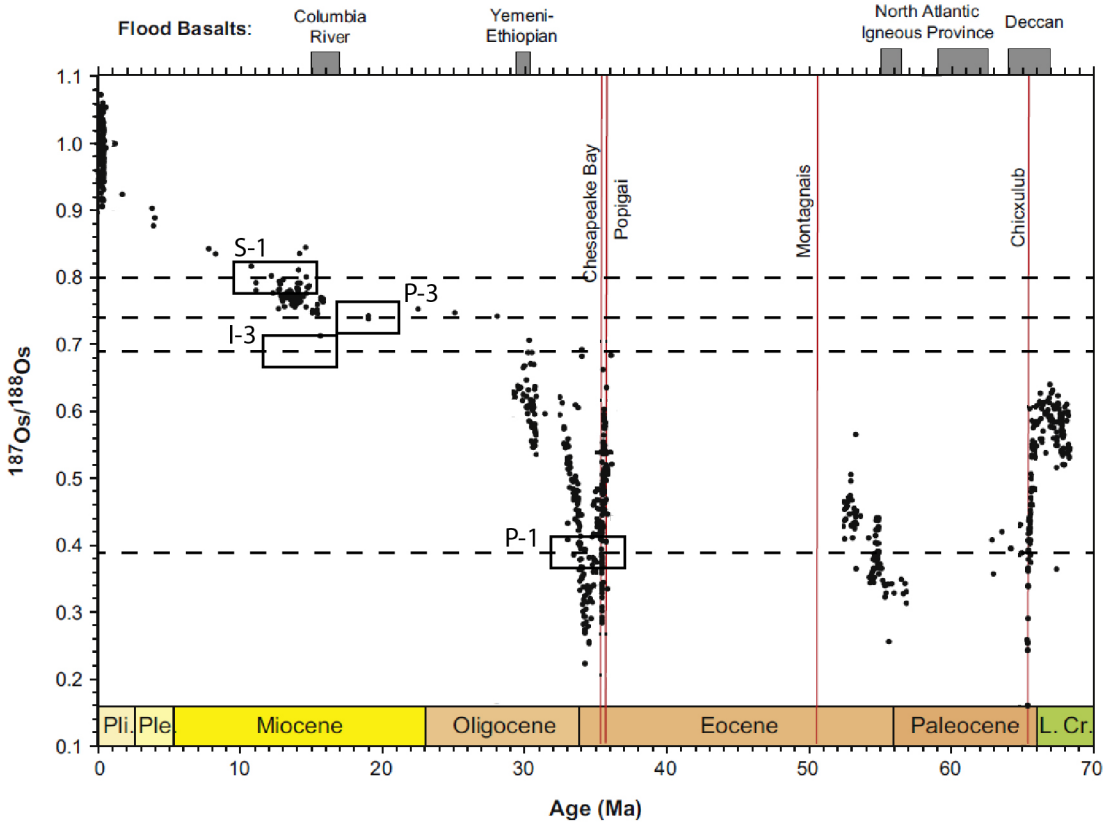

Figure 10 - Marine 187Os/188Os record of the past 70 million years, compiled by Peuker-Ehrenbrink & Ravizza (2012). 187Os/188Os values are used in this study to match the deposition of intervals of Maikop rock to the geologic record of seawater osmium to produce qualititative age dates and establish connectivity or restriction of basin waters to circulation to open marine waters. Dashed lines represent sample suite 187Os/188Os values for sample suites analyzes (Figure 2). Boxes represent interpreted qualitative ages of deposition.

The new constraints on deposition timing from Re-Os geochronology provides greater resolution on the rate of sedimentation in the Kura Basin. Sample suite I-1 was deposited at ~17.2 Ma, while suite I-3 is interpreted to have been deposited around the late Middle Miocene (~14 Ma; supported by conclusions from Popov et al., 2008). With less than 100 m between sample suites I-1 and I-3, sedimentation rates between these samples is about 2.5 cm/kyr. Low sedimentation rates may be due to a lack of sediment supply due to generally flat topography surrounding the Kura Basin during the time of Maikop deposition.

Low enrichment factors for detrital indicators also seem to suggest that sedimentation was low, as most of the samples showed relative depletion in detrital indicators. Two sample suites showed significant enrichment in detrital indicators: the Islamdag I-3 and Perikeshkul P-3 sites (enrichment average of 1.0-1.20 and 1.20-1.60 for Ti and Al, respectively), neither of which are reasonably stratigraphically correlatable. Their lack of stratigraphic correlation indicates that an allogenic event may have taken place to increase the detrital fraction of the rocks at these intervals. Possible allogenic events include volcanic events in the Talysh Mountains near the EOT during deposition of P-3, the initial uplift of the Greater Caucasus Mountains as a result of collisional tectonics in the mid-Miocene during deposition of sample suite I-1, and varying sediment source from or proximity to the paleo-Volga river to the north.

Current time constraints placing initial uplift of the Caucasus Mountains in the Middle Miocene are coincident with the deposition of the Islamdag I-1 sample suite, as indicated by isochron data. Initial uplift of the mountains from collisional tectonics paired with relative sea level change may have resulted in periods of increased restriction in the Kura Basin during deposition of the I-1 sample suite, resulting in the variable initial $^{187}Os/^{188}Os$ seawater value (from 0.8 ± 0.14 to 0.56 ± 0.13; Figure 8). Furthermore, exposure of earlier deposits of black shale may have resulted from the collisional tectonics or as a result of basin restriction and relative sea level fall, thereby allowing for the erosion and release of previously bound Os back into the basin. This may explain the anomalously high concentration of common Os in the Islamdag I-1 sample suite. Detrital input present in all of the Islamdag samples seems inconsistent with the emergence of the Greater Caucasus Mountains, as detrital indicators relatively increase at the I-1 suite, decrease in the I-2 suite, and then significantly increase in the I-3 suite. This variation may be the result of intermittent uplift of the Caucasus Mountains that

exposed fresh surfaces to erode and contribute higher amounts of nutrients, Os, and detrital silt. Restriction of the Kura and South Caspian Basins accompanied the initial emergence of the Caucasus Mountains, as indicated by the development of suboxic-anoxic bottom water conditions in the I-1 suite. Higher TOC values resulted from basin restriction in the I-1 sample suite. High TOC values in the S-2 suite may be the result of an increased amount of fresh nutrients being brought into the system as pelagic and solute load sourced from the newly uplifted and exposed soluble sedimentary minerals that were covering the now-emergent Greater Caucasus Mountains. After significant degradation and incision of young sedimentary units accompanied with further uplift of the Caucasus Mountains, harder, less nutrient-rich, less soluble minerals may have begun to erode that resulted in the increased fraction of detrital silt and lower TOC preserved in the I-3 suite.

Conclusions

The results from the studies performed by Hudson et al. (2008) and Johnson et al. (2009) indicate that the bulk of Maikop strata in the Kura Basin is not traditional deep-marine anoxic black shales with high TOC, but is rather primarily composed of gray shale with low, terrestrial-dominant organic matter. New data from this study confirm their conclusions and build upon the understanding of the important, but infrequent development of anoxia and the preservation of organic matter. The only intervals of high TOC with marine organic matter were from the middle and lower outcrops of Maikop taken from Mount Islamdag. The lower Islamdag sample suite was determined by Re-Os geochronology to have been deposited well into the Miocene (~17.2 Ma), thereby providing a datum of reference for future stratigraphy. As of yet, this is the

youngest age date produced from Re-Os geochronology. Variable Os_i and the production of two geochronologically identical (within uncertainty) isochrons in the lower Islamdag suite is likely the result of rapid, dynamic basin shifts not recorded in any other observed geochemical indicators. High values of common Os in the Islamdag I-1 suite suggest an efficient mechanism of Os delivery caused by the emergence of the Greater Caucausus Moutains and the subsequent exposure and weathering of Os-rich minerals, a more efficient uptake of Os into organic matter due to the higher fraction of marine organic material found in the samples or the development of suboxic to anoxic bottom-water conditions, or a combination of these factors.

Where Re-Os geochronology is not definitive, qualitiative age control of Maikopian strata was obtained by comparing $^{187}Os/^{188}Os$ values with the global $^{187}Os/^{188}Os$ sea level curve (Peucker-Ehrenbrink & Ravizza, 2012). The stratigraphically oldest strata studied, from just below what is commonly picked as the base of the Maikop Series, was found to be deposited near the Eocene-Oligocene Transition, as reflected by the $^{187}Os/^{188}Os$ excursion. This confirms the age proposed for the base of the Maikop Series in the Kura Basin to be after the Eocene-Oligocene Transition (Popov et al., 2008; Hudson et al., 2008). Time constraints on sample suites from Mount Islamdag revealed an average sedimentation rate of 2.5 cm/kyr. The low sedimentation rate of Maikop in these sections is likely due either to a lack of a highly emergent sediment source, changing provenance, or a combination of factors.

Comparisons of organic matter type and preservation, detrital input, indicators of anoxia, and correlation of $^{187}Os/^{188}Os$ ratios with the global sea record revealed that the basin was likely connected to open water circulation throughout the deposition of the Maikop units analyzed in this study (from the Eocene-Oligocene Transition through the late Middle Miocene). The causes of dysoxia/anoxia during the deposition of the Islamdag I-1 sample suite was probably related to

increased restriction of the Kura Basin due to collisional tectonics resulting in the emergence of the Greater Caucasus Mountains paired with asymmetric relative sea level rise and fall. Increased detrital input may be due to variations in sediment source cause by the emergence of the Greater Caucasus Mountains or due to changing proximity of sediment sources such as the Paleo-Volga River. Variation in sediment source may also have influenced the influx and radiogenic nature of Re and Os brought into the system.

References

ALGEO, T.J. and MAYNARD, J.B, 2004. Trace element behavior and redox facies in core shales of Upper Pennsylvanian Kansas-type cyclothems. Chem. Geol., 206, 289-318.

ALLEN, M.B., JONES, S., ISMAIL-ZADEH, A., SIMMONS, M., and ANDERSON, L., 2002. Onset of subduction as the cause of rapid Pliocene-Quaternary subsidence in the South Caspian Basin. Geology, 30, 775-778.

ALLEN, M.B., VINCENT, S.J., ALSOP, G.I., ISMAIL-ZADEH, A., and FLECKER, R., 2003. Late Cenozoic deformation in the South Caspian region: effects of a rigid basement block within a collision zone. Tectonophysics, 366, 223-239.

ARNDT, S., JØRGENSEN, B.B., LAROWE, D.E., MIDDELBURG, J.J., PANCOST, R.D., and REGNIER, P., 2013. Earth-Science Reviews, 123, 53-86.

BAIOUMY, H.M., EGLINTON, L.B., and PEUKER-EHRENBRINK, B., 2011. Rhenium-osmium isotope and platinum group element systematics of marine vs. non-marine organic-rich sediments and coals from Egypt. Chem. Geol., 285, 70-81.

BARNES, C.E., and COCHRAN, J.K., 1991. Geochemistry of uranium in Black Sea sediments. Deep Sea Research Part A. Oceanographic research Papers, 38, 1237-1254.

BECHTEL, A., MUVSUMOVA, U., PROSS, J., GRATZER, R., CORIC, S., and REINHARD, F.S., 2014. The Oligocene Maikop series of Lahich (eastern Azerbaijan): Paleoenvironment and oil-source rock correlation. Org. Geochem., 71, 43-59.

BERBERIAN, M., 1983. The southern Caspian: A compressional depression floored by a trapped, modified ocean crust. Canadian Journal of Earth Sciences, 20 (2), 163-183.

BRUNET, M.F., KOROTAEV, M.V., ERSHOV, A.V., and NIKISHKIN, A.M., 2003. The South Caspian Basin: a review of its evolution from subsidence modeling. Sedimentary Geology, 156, 119-148.

CALVERT, S.E., and PEDERSEN, T.F., 1993. Geochemistry of recent oxic and anoxic sediments: implications for the geological record. Mar. Geol., 113, 67-88.

CALVERT, S.E. and PEDERSEN, T.F., 1996. Sedimentary geochemistry of Manganese: Implications for the environment of formation of manganiferous black shales. Economic Geol., 91, 36-47.

COHEN, A.S., COE, A.L., BARTLETT, J.M., and HAWKESWORTH, C.J., 1999. Precise Re-Os ages of organic-rich mudrocks and the Os isotope composition of Jurassic seawater. Earth Planet. Sci. Lett., 167, 159-173.

COLODNER, D., SACHS., J., RAVIZZA, G., TUREKIAN, K.K., EDMOND, J., and BOYLE, E.A., 1993. The geochemical cycle of rhenium: a reconnaissance. Earth Planet. Sci. Lett., 117, 205-221.

CREASER, R.A., SANNIGRAHI, P., CHACKO, T., and SELBY, D., 2002. Further evaluation of the Re-Os geochronometer in organic-rich sedimentary rocks: A test of hydrocarbon maturation effects in Exshaw Formation, Western Canada Sedimentary Basin. Geochim. Cosmochim. Acta, 66, 3341-3452.

CRUSIUS, J., CALVERT, S., PEDERSEN, T., and SAGE, D., 1996. Rhenium and molybdenum enrichments in sediments as indicators of oxic, suboxic, and sulfidic conditions of deposition. Earth Planet. Sci. Lett., 145, 65-78.

CUMMING, V.M., SELBY, D., and LILLIS, P.G., 2012. Re-Os geochronology of the lacustrine Green River Formation: Insights into direct depositional dating of lacustrine successions, Re-Os systematics and paleocontinental weathering. Earth Planet. Sci. Lett., 359-360, 194-205.

DALAI, T.K., RAVIZZA, G., and PEUCKER-EHRENBRINK, B., 2006. The Late Eocene 187Os/188Os excursion: Chemostratigraphy, cosmic dust flux and the early Oligocene glaciation. Earth Planet. Scie. Lett., 241, 477-492.

DERCOURT, J., ZONENSHAIN, L.P., RICOU, L.E., KAZMIN, V.G., LEPICHON, X.L., KNIPPER, A.L., GRANDJACQUET, C., SBORTSHIKOV, I.M., GEYSSANT, J., LEPVRIER, C., PECHERSKY, D.H., BOULIN, J., SIBUET, J.-C., SAVOSTI, L.A., SOROKHTIN, O., WESTPHAL, M., BAZHENOV, M.L., LAUER, J.P., and BIJU-DUVAL, B., 1986. Geological evolution of the tethys belt from the atlantic to the pamirs since the LIAS. Tectonophysics, 123, 241-315.

DICKIN, A.P., 2008. Radiogenic Isotope Geology. Cambridge University Press, Cambridge.

EFENDIYEVA, M., BABAEV, R., JOHNSON, C., FEYZULLAYEV, A., and ALIEV, C., 2012. Radiostratigraphic Study of the Deposits of the Maikop Group, Western Azerbaijan. Stratigraphy and Geological Correlation, 20, 567-577.

ERSHOV, A. V., BRUNET, M. F., NIKISHIN, A. M., BOLOTOV, S. N., NAZAREVICH, B. P., & KOROTAEV, M. V., 2003. Northern Caucasus basin: thermal history and synthesis of subsidence models. Sedimentary Geology, 156(1-4), 95-118.

FERNEX, F., FÉVRIER, G., BENAÏM, J., and ARNOUX, A., 1992. Copper, lead and zinc trapping in Mediterranean deep-sea sediments: probable coprecipitation with manganese and iron. Chem. Geol. 98, 293-308.

GAETANI, M., and GARZANTI, E., 1991. Multicyclic history of the northern India continental margin (northwestern Himalaya). AAPG Bulletin, 75, 1427-1446.

GEORGIEV, S., STEIN, H.J., HANNAH, J.L., BINGEN, B., WEISS, H.M., and PIASECKI, S., 2011. Hot acidic Late Permian seas stifle life in record time. Earth Planet. Sci. Lett., 310, 389-400.

GEORGIEV, S., STEIN, H.J., HANNAH, J.L., WEISS, H.M., BINGEN, B., XU, G., REIN, E., HATLØ, V., LØSETH, H., NALI, M., and PIASECKI, S., 2012. Chemical signals for oxidative weathering predict Re-Os isochroneity in black shales, East Greenland. Chem. Geol., 324-325, 108-121.

GOLONKA, J. (2004) Plate tectonic evolution of the southern margin of Eurasia in the Mesozoic and Cenozoic. Tectonophysics, 381, 235-273.

GOTH, K., DE LEEUW, J.W., PÜTTMANN, W., and TEGELAAR, E.W., 1988. Origin of Messel oil shale kerogen. Nature, 336, 759-761.

GRANATH, J.W., and BAGANZ, O.W., 1996. A review of Neogene subsidence mechanisms for the South Caspian Basin. 3rd Annual Meeting and Fieldtrip of IGCP Project n °369 "Comparative evolution of Peri-Tethyan rift basins", Centennial Celebration of EGSMA, November 19-24, Cauro, Egypt, 24-25.

GRANATH, J.W., SOOFI, K.A., BAGANZ, O.W., and BAGIROV, E., 2000. Gravity modeling and its implications to the tectonics of the South Caspian Basin [Abstract]. Istanbul 2000, AAPG's Inaugural Regional International Conference, July 9-12, 2000. Istanbul, Turkey, 46-49.

GREEN, T., ABDULLAYEV, N., HOSSACK, J., RILEY, G., and ROBERTS, A.M., 2009. Sedimentation and subsidence in the South Caspian Basin, Aerbaijan. The Geological Society of London, Special Publications, 312, 241-260.

HARRIS, N.B., MNICH, C.A., SELBY, D., and KORN, D., 2013. Minor and trace element and Re-Os chemistry of the Upper Devonian Woodford Shale, Permian Basin, west Texas: Insights into metal abundance and basin processes. Chem. Geol., 359, 76-93.

HEDGES, J.I., KEIL, R.G., and BENNER, R., 1997. What happens to terrestrial organic matter in the ocean? Org. Geochem., 27, 195-212.

HUDSON, S.M., JOHNSON, C.L., EFENDIYEVA, M.A., ROWE, H.D., FEYZULLAYEV, A.A., and ALIYEV, C.S., 2008. Stratigraphy and geochemical characterization of the Oligocene-Miocene Maikop series: implications for the paleogeography of Eastern Azerbaijan. Tectonophysics, 451, 40-55.

HUDSON, S.M., JOHNSON, C.L., and AFANDIYEVA, M.A., 2016. Spatial and temporal variability of Paleocene-Miocene organofacies of the Kura Basin, eastern Azerbaijan, and implications for basin evolution and petroleum generation. Org. Geochem., 97, 131-147.

HUERTA-DIAZ, M.A., and MORSE, J.W., 1992. Pyritisation of trace metals in anoxic marine sediments. Geochim. Cosmochim., 56, 2681-2702.

HUGUET, C., DE LANGE, G.J., GUSTAFSSON, O., MIDDELBURG, J.J., DAMASTÉ, J.S.S., and SCHOUTEN, S., 2008. Selective preservation of soil organic matter in oxidized marine sediments (Madeira Abyssal Plain). Geochim. Cosmochim. Acta, 72, 6061-6068.

INGAMELLS, C.O., 1970. Lithium metaborate flux in silicate analysis. Analytica Chimica Acta, 52, 323-334.

ISAKSEN, G.H., ALIYEV, A., BARBOZA, S.A., PULS, D., and GULIYEV, I., 2007. Regional evaluation of source rock wuality in Azerbaijan from the geochemistry of organic-rich rocks in mud-volcano ejecta. In: YILMAZ, P.O., and ISAKSEN, G.H., (Eds.): Oil and gas of the Greater Caspian area. AAPG Studies in Geology., 55, 51-64.

JACOT DES COMBES, H., CAULET, J.P., and TRIBOVILLARD, N., 1999. Pelagic productivity changes in the equatorial area of the NW Indian Ocean during the last 400 kyr. Mar. Geol., 158, 27-55.

JOHNSON, C.L., HUDSON, S.M., ROWE, H.D., and EFENDIYEVA, M.A., 2009. Geochemical constraints on the Paleocene-Miocene evolution of eastern Azerbaijan, with implications for the South Caspian basin and eastern Paratethys. Basin Research, 22, 735-755.

KAZ'MIN, V.G., and TIKHONOVA, N.F., 2006. Late Cretaceous-Eocene marginal seas in the Black Sea - Caspian Region: Paleotectonic reconstructions. Geotectonics, 40, 169-182.

KENDALL, B., CREASER, R.A., SELBY, D., 2009. 187Re-187Os geochronology of Precambrian organic-rich sedimentary rocks. Geol. Soc. London, Special Publications, 326, 85-107.

KLINKHAMMER, G.P., and PALMER, M.R., 1991. Uranium in the oceans: where it goes and why. Geochim. Cosmochim., 55, 1799-1806.

KRYC, K.A., MURRAY, R.W., and MURRAY, D.W., 2003. Elemental fractionation of Si, Al, Ti, Fe, Ca, Mn, P, and Ba in five marine sedimentary reference materials: results from sequential extractions. Anal. Chim., 487, 117-128.

LANGUIMER, D., 1978. Uranium solution-mineral equilibria at low temperatures with applications to sedimentary ore deposits. Geochim. Cosmochim. Acta, 42, 547-569.

MCARTHUR, J.M., ALGEO, T.J., VAN DE SCHOOTBRUGGE, B., LI, Q., and HOWARTH, R.J., 2008. Basinal restriction, black shales, Re-Os dating, and the Early Toarcian (Jurassic) oceanic anoxic event. Paleoceanography, 23, doi:10.1029/2008PA001607.

MCMANUS, J., BERELSON, W.M., KLINKHAMMER, G.P., HAMMOND, D.E., and HOLM, C., 2005. Authigenic uranium: relationship to oxygen penetration depth and organic carbon rain. Geochim. Cosmochim., 69, 95-108.

MORFORD, J.L., and EMERSON, S., 1999. The geochemistry of redox sensitive trace metals in sediments. Geochim. Cosmochim., 63, 1735-1750.

NAMEROFF, T.J., BALISTRIERI, L.S., and MURRAY, J.W., 2002. Suboxic trace metal geochemistry in the eastern tropical North Pacific. Geochim. Cosmochim., 66, 1139-1158.

NAMEROFF, T.J., CALVERT, S.E., and MURRAY, J.W., 2004. Glacial-interglacial variability in the eastern tropical North Pacific oxygen minimum zone recorded by redox-sensitive trace metals. Paleoceanography 19, PA 1010. doi:10.1029/2003PA000912.

NARIMANOV, A.A., 1993. The petroleum systems of the South Caspian Basin. In: DORÉ, A.G. et al. (Eds.): Basin Modeling: Advances and Applications, 559-608.

NIKISHIN, A.M., BRUNET, M.-F., STEPHENSON, R., and BOLOTOV, S.N., 1998. Scythian Platform, Caucasus and Black Sea region: Mesozoic-Cenozoic tectonic history and dynamics. In: CRASQUIN-SOLEAU, S., and BARRIER, É., (Eds.): Peri-Tethys Memoir 3: stratigraphy and evolution of Peri-Tehtyan platforms. Mem. Mus. natn. Hist. nat., 177, 163-176.

OTTO, S.C., 1997. Mesozoic-Cenozoic history of deformation and petroleum systems in sedimetnary basins of Central Asia; implications of collisions on the Eurasian margin. Petroleum Geoscience, 3, 327-341.

PETERS, K.E., 1986. Guidelines for evaluating petroleum source rock using programmed pyrolysis. AAPG Bulletin, 3, 318-329.

PEUCKER-EHRENBRINK, B., and RAVIZZA, G., 2012. Osmium isotope stratigraphy. In: GRANDSTEIN, F.M., OGG, J.G., SCHMITZ, M., and OGG, G. (Eds.): The Geologic Time Scale. DOI: 10.1016/B978-0-444-59425-9.000008-1

PIERSON-WICKMAN, A.C., REISBERG, L., and FRANCE-LANORD, C., 2000. The Os isotopic composition of Himalayan river bedloads and bedrocks: Importance of black shales. Earth Planet. Sci. Lett., 176, 203-218.

PIPER, D.Z., and PERKINS, R.B., 2004. A modern vs. Permian black shale - the hydrography, primary productivity, and water-column chemistry of deposition. Chem. Geol. 206, 177-197.

POPOV, S.V., VORONINA, A.A., and GONCHAROVA, I.A., 1993. Stratigraphy and bivalves of the Oligocene-Lower Miocene of the Eastern Paratethys. Inst. Ross. Akad. Nauk,

POPOV, S.V., SYCHEVSKAYA, E.K., AKHMET'EV, M.A., ZAPOROZHETS, N.I., and GOLOVINA, L.A., 2008. Stratigraphy of the Maikop Group and pteropoda beds in Northern Azerbaijan. Strat. and Geol.Corr., 16, 664-677.

PRIESTLEY, K., BAKER, C., and JACKSON, J. (1994). Implications of earthquake focal mechanism data for the active tectonics of the South Caspian Basin and surrounding regions. Geophysical Journal International, 118(1), 111-141.

RACIONERO-GOMEZ, B., SPROSON, A.D., SELBY, D., GANNOUN, A., GROCKE, D.R., GREENWELL, H.C., and BURTON, K.W., 2017. Osmium uptake, distribution and 187Os/188Os and 187Re/188Os compositions in Phaephyceae macroalgae, Fucus vesiculosus: implications for determining the 187Os/188Os composition of seawater. Geochim. Cosmochim., 199, 48-57.

RAVIZZA, G., and ESSER, B.K., 1993. A possible link between the seawater osmium isotope record and weathering of ancient sedimentary organic matter. Chem. Geol., 107, 255-258.

RAVIZZA, G., and TUREKIAN, K.K., 1989. Application of the 187Re-187Os system to black shale geochronometry. Geochim. Cosmochim., 53, 3257-3262.

RAVIZZA, G., and TUREKIAN, K.K., 1992. The osmium isotopic composition of organic-rich marine sediments. Earth and Planetary Science Letters, 110, 1-6.

RAVIZZA, G., and TUREKIAN, K.K., 2012. The Os isotopic composition of organic-rich marine sediments. Earth Planet. Sci. Lett., 110, 1-6.

RAVIZZA, G., TUREKIAN, K.K., and HAY, B.J., 1991. The geochemistry of rhenium and osmium in recent sediments from the Black Sea. Geochim. Cosmochim., 55, 3741-3752.

ROGL, F., 1999. Mediterranean and Paratethys - facts and hypotheses of an Oligocene to Miocene paleogeography (short overview). Geologica Carpathica, 50, 339-349.

ROONEY, A.D., SELBY, D., HOUZAY, J.P., and RENNE, P.R., 2010. Re-Os geochronology of a Mesoproterozoic sedimentary succesion, Taoudeni basin, Mauritania: implications for basin-wide correlations and Re-Os organic-rich sediments systematics. Earth Planet. Sci. Lett., 289, 486-496.

ROONEY, A.D., SELBY, D., LEWAN, M.D., LILLIS, P.G., and HOUZAY, J.P., 2012. Evaluating Re-Os systematics in organic-rich sedimentary rocks in response to petroleum generation using hydrous pyrolysis experiments. Geochim. Cosmochim. Acta, 77, 275-291.

ROONEY, A.D., SELBY, D., LLOYD, J.M., ROBERTS, D.H., LÜCKGE, A., SAGEMAN, B.B., and PROUTY, N.G., 2016. Tracking millenial-scale Holocene glacial advance and retreat using osmium isotopes: Insights from the Greenland ice sheet. Quat. Sci. Reviews, 138, 49-61.

ROONEY, A.D., CHEW, D.M., and SELBY, D., 2011. Re-Os geochronology of the Neoproterozoic-Cambrian Dalradian Supergroup of Scotland and Ireland: Implications for Neoproterozoic stratigraphy, glaciations and Re-Os systematics. Precambrian Research, 185, 202-214.

SAINTOT, A., BRUNET, M-F., YAKOVLEV, F., SEBRIER, M., STEPHENSON, R., ERSHOV, A., CHALOT-PRAT, F., and MCCANN, T., 2006. The Mesozoic-Cenozoic tectonic evolution of the Greater Caucasus. London Geological Society, 32, 277-289.

SELBY, D., and CREASER, R.A., 2003. Re-Os geochronology of organic rich sediments: an evaluation of organic matter analysis methods. Chem. Geol., 200, 225-240.

SHARMA, M., ROSENBERG, E.J., and BUTTERFIELD, D.A., 2007. Search for the proverbial mantle osmium sources to the oceans: Hydrothermal alteration of mid-ocean ridge basalt. Geochim. et Cosmochim. Acta, 71 (19), 4655-4667.

SINGH, S.K., TRIVEDI, J.R., and KRISHNASWAMI, S., 1999. Re-Os isotope systematics in black shales from the Lesser Himalaya: their chronology and role in the $^{187}Os/^{188}Os$ evolution of seawater. Geochim. et Cosmochim. Acta, 63 (16), 2381-2392.

STAMPFLI, G.M., BOREL, G.D., CAVAZZA, W., MOSAR, J., and ZIEGLER, P.A., 2001. Palaeotectonic and palaeogeographic evolution of the western Tethys and PeriTethyan domain. Episodes, 24 (4), 222.

TRIBOVILLARD, N., ALGEO, T.J., LYONS, T., and RIBOULLEAU, A., 2006. Trace metals as paleoredox and paleoproductivity proxies: an update. Chem Geol., 232, 12-32.

VAN DER BOON, A., KUIPER, K.F., VILLA, G., RENEMA, W., MEIJERS, M.J.M., LANGEREIS, C.G., ALIYEVA, E., and KRIJGSMAN, W., 2015. Onset of Maikop sedimentation and cessation of Eocene arc volcanism in the Talysh Mountains, Azerbaijan. In: SOSSON, M., STEPHENSON, R.A., and ADAMIA, S.A. (Eds.): Tectonic evolution of the Eastern Black Sea and Caucasus. Geological Society, London, Special Publications, 428, DOI: 10.1144/SP428.3

VINCENT, S.J., MORTON, A.C., CARTER, A., GIBBS, S., and BARABADZE, T.G., 2007. Oligocene uplift of the Western Greater Caucasus: an effect of initial Arabia-Eurasia collision. Terra Nova, 19, 160-166.

VOLKENIN, J., WALCZYK, T., and HEUMANN, K.G., 1991. Osmium isotope ratio determinations by negative thermal ionization mass spectrometry. International Journal of Mass Spectrometry and Ion Processes, 105 (2), 147-159.

WIJSMAN, J.W.M., MIDDELBURG, J.J., and HEIP, C.H.R., 2001. Reactive iron in Black Sea sediments: implications for iron cycling. Mar. Geol., 172, 167-180.

WOOD, S.A., and SAMSON, I.M., 2006. The aquesous geochemistry of gallium, germanium, indium and scandium. Ore Geology Reviews, 28, 57-102.

YAMASHITA, Y., TAKAHASHI, Y., HABA, H., ENOMOTO, S., and SHIMIZU, H., 2007. Comparison of reductive accumulation of Re and Os in seawater-sediment systems. Geochim. Cosmochim., 71, 3485-3475.

ZHENG, Y., ANDERSON, R.F., VAN GREEN, A., and FLEISHEIR, M.Q., 2002a. Preservation of non-lithogenic particulate uranium in marine sediments. Geochim. Cosmochim., 66, 3085-3092.

ZHENG, Y., ANDERSON, R.F., VAN GREEN, A., and FLEISHEIR, M.Q., 2002b. Remobilizaiton of authigenic uranium in marine sediments by bioturbation. Geochim. Cosmochim., 66, 1759-1772.

ZEIGLER, P.A., CLOETHINGH, S., GUIRAUD, R., and STAMPFLI, G.M., 2001. Peri-Tethyan platforms: constraints on dynamics of rifting and basin inversion. In: ZIEGLER, P.A., CAVAZZA, W., ROBERTSON, A.H.F., and CRASQUIN-SOLEAU, S., (eds) Peri-Tethys Memoir 6: Peri-Tethyan Rift/Wrench Basins and Passive Margins. Memoires du Museum national d/Histoire naturelle, Paris, 186, 9-49.

ZONENSHAIN, L.P., and LE PICHON, X., 1986. Deep basins of the Black Sea and Caspian Sea as remnants of Mesozoic back arc basin. Tectonophysics, 123, 181-211.

Sample Suite	Value	S1-Free Oil (mgHC/g rock)	S2-Kerogen Yield (mgHC/g rock)	S3 (mgCO2/g rock)	Tmax-Maturity (°C)	TOC-Total Organic Carbon (Weight %)	CC-Carbonate Carbon (Weight %)	GOC-Generative OC (Weight %)	NGOC-Non-generative OC (Weight %)	AI-Adsorption Index (Weight %)	OSI-Oil Sat.Index (mgHC/gTOC)	PI-Production Index	HI-Hydrogen Index (mgHC/gTOC)	OI-Oxygen Index (mgCO2/gTOC)
Islamdag	Average	0.33	8.22	0.56	421.80	2.29	0.13	0.77	1.53	1.88	11.36	0.07	265.48	39.44
	Min	0.03	0.15	0.27	402.00	0.58	0.10	0.04	0.53	0.48	3.00	0.03	24.00	11.00
	Max	1.00	28.44	0.96	434.00	4.58	0.22	2.55	2.89	3.76	21.00	0.29	620.00	125.00
I-3	Average	0.04	0.22	0.57	431.88	0.68	0.13	0.05	0.63	0.56	5.13	0.15	31.88	84.38
	Min	0.03	0.15	0.37	430.00	0.58	0.10	0.04	0.53	0.48	3.00	0.10	24.00	58.00
	Max	0.08	0.31	0.76	434.00	0.83	0.17	0.06	0.78	0.68	12.00	0.29	41.00	125.00
I-2	Average	0.56	15.47	0.45	427.33	2.99	0.12	1.40	1.59	2.46	17.44	0.04	481.33	15.89
	Min	0.23	4.70	0.27	425.00	1.47	0.10	0.45	1.02	1.21	15.00	0.03	319.00	11.00
	Max	1.00	28.44	0.60	431.00	4.58	0.16	2.55	2.04	3.76	21.00	0.05	620.00	32.00
I-1	Average	0.35	8.06	0.68	405.50	3.12	0.14	0.77	2.35	2.56	10.75	0.04	256.25	21.00
	Min	0.28	6.19	0.52	402.00	2.67	0.11	0.60	2.05	2.19	10.00	0.04	231.00	17.00
	Max	0.50	10.38	0.96	408.00	3.82	0.22	1.00	2.89	3.14	13.00	0.05	299.00	25.00
Perikeshkul	Average	0.04	0.14	0.72	378.47	0.64	1.64	0.05	0.59	0.52	6.63	0.35	17.68	153.05
	Min	0.01	0.01	0.24	341.00	0.18	0.07	0.02	0.16	0.15	1.00	0.12	3.00	36.00
	Max	0.09	0.51	1.23	424.00	2.45	8.27	0.10	2.36	2.01	14.00	0.57	47.00	271.00
P-3	Average	0.09	1.05	0.77	429.75	1.28	0.10	0.14	1.14	1.05	6.75	0.08	80.50	60.25
	Min	0.06	0.68	0.60	428.00	0.99	0.06	0.09	0.89	0.81	6.00	0.07	61.00	49.00
	Max	0.12	1.50	0.86	431.00	1.49	0.17	0.17	1.31	1.22	8.00	0.10	100.00	69.00
P-2	Average	0.01	0.01	0.35	359.60	0.21	0.10	0.03	0.19	0.18	5.20	0.47	6.40	165.00
	Min	0.01	0.01	0.24	344.00	0.18	0.07	0.02	0.16	0.15	4.00	0.37	5.00	134.00
	Max	0.01	0.02	0.43	397.00	0.25	0.12	0.03	0.22	0.21	6.00	0.53	11.00	221.00
P-1	Average	0.07	0.29	1.05	393.67	0.90	1.80	0.07	0.83	0.74	8.56	0.23	31.00	151.44
	Min	0.05	0.10	0.87	366.00	0.36	0.83	0.05	0.31	0.30	3.00	0.12	20.00	41.00
	Max	0.09	0.51	1.23	419.00	2.45	2.29	0.10	2.36	2.01	14.00	0.35	47.00	264.00
Shikhzahirli	Average	0.08	1.80	0.47	421.00	0.99	0.40	0.19	0.80	0.81	7.71	0.06	164.00	51.75
	Min	0.03	0.22	0.27	413.00	0.39	0.07	0.05	0.35	0.32	4.00	0.03	54.00	24.00
	Max	0.14	3.24	0.79	429.00	1.39	0.89	0.32	1.09	1.14	12.00	0.12	248.00	113.00
S-3	Average	0.04	0.71	0.50	421.25	0.67	0.37	0.09	0.57	0.55	5.88	0.07	101.38	77.13
	Min	0.03	0.22	0.36	417.00	0.39	0.24	0.05	0.35	0.32	4.00	0.03	54.00	52.00
	Max	0.06	1.69	0.63	424.00	0.89	0.57	0.18	0.74	0.73	7.00	0.12	189.00	113.00
S-2	Average	0.10	1.78	0.38	414.88	1.02	0.12	0.19	0.83	0.84	9.88	0.07	163.25	38.13
	Min	0.08	0.73	0.27	413.00	0.75	0.07	0.10	0.66	0.62	7.00	0.04	97.00	29.00
	Max	0.14	3.09	0.52	417.00	1.39	0.15	0.31	1.09	1.14	12.00	0.10	235.00	51.00
S-1	Average	0.10	2.92	0.52	426.88	1.28	0.72	0.29	0.99	1.05	7.38	0.03	227.38	40.00
	Min	0.09	2.58	0.32	425.00	1.23	0.53	0.26	0.95	1.01	7.00	0.03	194.00	24.00
	Max	0.11	3.24	0.79	429.00	1.33	0.89	0.32	1.07	1.09	8.00	0.04	248.00	62.00

Table 1 - Average results from HAWK pyrolysis by sample location and sample suite. Stratigraphically, suite 1 represents the oldest sampled unit at the sample location, and 3 the youngest. Pyrolysis results reveal a generally low TOC for Maikop samples in the Kura Basin. Organic matter type is derived from Oxygen Index (OI) and Hydrogen Index (HI), while maturity is derived from Tmax values.

Table 2

Batch/Sample	Re (ppb)	±	Os (ppt)	±	^{192}Os (ppt)	±	^{187}Re/^{188}Os	±	^{187}Os/^{188}Os	±	rho	% Re Blank	% ^{187}Os Blank	% ^{188}Os Blank	Osi @ XX myr	±
I-1 (1)	314.5	0.8	585.2	2.7	200.7	0.7	3117.1	13.7	1.689	0.009	0.579	0.013	0.010	0.067	0.80	0.01
I-1 (2)	376.4	0.9	489.3	2.3	163.4	0.6	4583.6	19.6	1.940	0.010	0.581	0.011	0.010	0.082	0.63	0.02
I-1 (3)	421.7	1.0	453.9	2.3	144.2	0.5	5817.4	25.8	2.423	0.012	0.589	0.009	0.010	0.093	0.76	0.02
I-1 (4)	412.6	1.0	598.8	2.7	202.7	0.7	4048.5	17.3	1.809	0.009	0.577	0.010	0.009	0.066	0.65	0.01
I-1 (5)	111.3	0.3	300.8	1.3	106.9	0.4	2070.6	9.2	1.365	0.007	0.601	0.036	0.023	0.125	0.77	0.01
I-1 (6)	167.2	0.4	437.9	1.7	158.5	0.6	2098.8	9.0	1.205	0.006	0.585	0.024	0.017	0.084	0.60	0.01
I-1 (7)	413.9	1.0	442.9	2.2	141.8	0.5	5806.5	25.2	2.345	0.012	0.583	0.010	0.010	0.094	0.68	0.02
I-1 (8)	313.1	0.8	450.7	2.2	149.7	0.6	4161.1	18.6	1.992	0.011	0.567	0.013	0.011	0.089	0.80	0.02
Average	316.3		469.9		158.5	0.6						0.016	0.013	0.088	0.71	
S-1 (1)	14.34	0.04	134.5	0.5	49.9	0.2	572.3	2.8	0.998	0.006	0.630	0.03	0.04	0.16	0.83	0.01
S-1 (2)	13.19	0.03	137.2	0.6	51.0	0.2	514.8	2.5	0.983	0.006	0.621	0.04	0.04	0.16	0.84	0.01
S-1 (3)	15.79	0.04	136.4	0.6	50.5	0.2	621.8	3.0	1.003	0.006	0.626	0.03	0.04	0.16	0.83	0.01
S-1 (4)	15.99	0.04	136.7	0.6	50.7	0.2	627.9	3.1	0.998	0.006	0.616	0.03	0.04	0.16	0.82	0.01
S-1 (5)	14.99	0.04	138.1	0.6	51.2	0.2	582.8	2.8	0.999	0.006	0.625	0.03	0.04	0.16	0.83	0.01
S-1 (6)	17.55	0.04	138.6	0.6	51.4	0.2	679.2	3.3	0.994	0.006	0.624	0.03	0.04	0.16	0.80	0.01
S-1 (7)	15.12	0.04	130.8	0.6	48.5	0.2	620.3	3.3	0.999	0.007	0.645	0.03	0.04	0.17	0.82	0.01
S-1 (8)	13.49	0.03	172.3	0.6	65.6	0.3	408.9	1.9	0.767	0.004	0.610	0.04	0.04	0.12	0.65	0.00
Average	15.06		140.56		52.34	0.22						0.032	0.040	0.155	0.80	
P-3 (1)	2.27	0.01	199.5	1.2	75.5	0.7	59.9	0.6	0.821	0.010	0.667	0.53	0.02	0.05	0.80	0.01
P-3 (2)	2.01	0.01	176.9	1.1	67.3	0.6	59.3	0.5	0.783	0.010	0.677	0.60	0.02	0.06	0.77	0.01
P-3 (3)	1.48	0.00	150.3	0.9	57.2	0.5	51.6	0.5	0.778	0.010	0.673	0.81	0.02	0.07	0.76	0.01
P-3 (4)	1.50	0.00	156.1	0.9	59.5	0.5	50.0	0.5	0.771	0.009	0.674	0.80	0.02	0.07	0.76	0.01
P-3 (5)	2.54	0.01	202.0	1.2	76.9	0.7	65.8	0.6	0.774	0.010	0.678	0.47	0.02	0.05	0.76	0.01
P-3 (6)	1.98	0.01	169.3	1.0	64.4	0.6	61.2	0.6	0.779	0.010	0.675	0.61	0.02	0.06	0.76	0.01
P-3 (7)	1.63	0.00	165.3	1.0	63.1	0.6	51.5	0.5	0.752	0.009	0.674	0.74	0.02	0.06	0.74	0.01
P-3 (8)	2.36	0.01	227.0	1.3	88.7	0.8	52.9	0.5	0.561	0.007	0.678	0.51	0.02	0.05	0.55	0.01
Average	1.97		180.80		69.07	0.60						0.63	0.02	0.06	0.74	
I-3 (1)	1.08	0.00	146.21	0.98	56.1	0.6	38.4	0.4	0.708	0.011	0.674	1.11	0.02	0.07	0.70	0.01
I-3 (2)	1.33	0.01	165.71	1.13	64.0	0.7	41.3	0.6	0.654	0.011	0.475	0.90	0.02	0.06	0.64	0.01
I-3 (3)	1.12	0.00	125.07	0.85	48.0	0.5	46.5	0.5	0.709	0.011	0.676	1.07	0.03	0.08	0.70	0.01
I-3 (4)	1.31	0.00	130.92	0.71	50.1	0.4	51.9	0.4	0.734	0.008	0.650	0.92	0.02	0.08	0.72	0.01
I-3 (5)	1.47	0.00	152.00	0.78	58.8	0.4	49.8	0.4	0.649	0.007	0.658	0.82	0.02	0.07	0.63	0.01
I-3 (6)	1.22	0.00	146.84	0.77	56.2	0.4	43.2	0.3	0.725	0.008	0.656	0.98	0.02	0.07	0.71	0.01
I-3 (7)	1.04	0.00	280.48	1.24	112.1	0.8	18.5	0.1	0.377	0.004	0.648	1.15	0.02	0.04	0.37	0.00
I-3 (8)	0.95	0.00	116.75	0.62	44.8	0.3	42.1	0.3	0.718	0.008	0.640	1.27	0.03	0.09	0.71	0.01
Average	1.19		158.00		61.26	0.52						1.03	0.02	0.07	0.69	0.01
P-1 (1)	5.71	0.01	213.15	0.61	84.4	0.3	134.5	0.6	0.456	0.002	0.581	0.21	0.02	0.05	0.42	0.00
P-1 (2)	10.63	0.03	276.93	0.83	109.6	0.4	192.9	0.9	0.459	0.003	0.594	0.11	0.02	0.04	0.40	0.00
P-1 (3)	9.85	0.02	518.20	1.46	209.0	0.9	93.8	0.5	0.310	0.002	0.600	0.12	0.01	0.02	0.28	0.00
P-1 (4)	8.37	0.02	275.89	0.90	108.9	0.5	152.9	0.8	0.478	0.003	0.608	0.14	0.02	0.04	0.44	0.00
P-1 (5)	6.45	0.02	259.83	0.95	103.0	0.5	124.5	0.7	0.445	0.003	0.636	0.19	0.02	0.04	0.41	0.00
P-1 (6)	19.30	0.05	267.91	0.76	106.1	0.4	361.8	1.6	0.450	0.002	0.577	0.06	0.02	0.04	0.35	0.00
P-1 (7)	13.19	0.03	324.43	0.99	128.5	0.5	204.2	1.0	0.450	0.003	0.594	0.09	0.02	0.03	0.39	0.00
P-1 (8)	6.17	0.02	196.90	0.73	77.9	0.4	157.7	0.9	0.464	0.003	0.638	0.19	0.02	0.05	0.42	0.00
Average	9.96		291.65		115.92	0.49						0.14	0.02	0.04	0.39	

Table 2. Synopsis of Re-Os data for the five sample suites as shown in Figure 8.